

Balance between senescence and apoptosis is regulated by telomere damage–induced association between p16 and caspase-3

Shanmugam Panneer Selvam<sup>1,2</sup>, Braden M. Roth<sup>1,2</sup>, Rose Nganga<sup>1,2</sup>, Jisun Kim<sup>1,2</sup>, Marion A. Cooley<sup>3,#</sup>, Kristi Helke<sup>4</sup>, Charles D. Smith<sup>5</sup>, and Besim Ogretmen<sup>1,2\*</sup>

<sup>1</sup>Department of Biochemistry and Molecular Biology, <sup>2</sup>Hollings Cancer Center, <sup>3</sup>Department of Regenerative Medicine, <sup>4</sup>Department of Comparative Medicine, Medical University of South Carolina, 86 Jonathan Lucas Street, Charleston, SC 29425; <sup>5</sup>Department of Pharmacology, Pennsylvania State University, 500 University Drive, Hershey, PA 17033.

#Current Address: Department of Oral Biology, Augusta University, Augusta, GA 30912.

\*Address correspondence to: [ogretmen@musc.edu](mailto:ogretmen@musc.edu)

Running title: p16-caspase-3 complex and senescence

Key words: apoptosis; senescence; sphingolipid; sphingosine 1-phosphate; telomere damage

## Abstract

Telomerase activation protects cells from telomere damage by delaying senescence and inducing cell immortalization, whereas telomerase inhibition mediates rapid senescence or apoptosis. However, the cellular mechanisms that determine telomere damage–dependent senescence versus apoptosis induction are largely unknown. Here, we demonstrate that telomerase instability mediated by silencing of sphingosine kinase 2 (SPHK2) and sphingosine 1-phosphate (S1P), which binds and stabilizes telomerase, induces telomere damage–dependent caspase-3 activation and apoptosis, but not senescence, in p16-deficient lung cancer cells or tumors. These outcomes were prevented by knockdown of a tumor-suppressor protein, transcription factor 21 (TCF21), or by ectopic expression of WT human telomerase reverse transcriptase (hTERT), but not mutant hTERT with altered S1P binding. Interestingly, SphK2-deficient mice exhibited accelerated aging and telomerase instability that increased telomere damage and senescence via p16 activation especially in testes tissues, but not in apoptosis. Moreover, p16 silencing in SphK2<sup>-/-</sup> mouse embryonic fibroblasts activated caspase-3 and apoptosis without inducing senescence. Further, ectopic WT p16 expression in p16-deficient A549 lung cancer cells prevented TCF21 and caspase-3 activation, and resulted in senescence in response to SphK2/S1P inhibition and telomere damage. Mechanistically, a p16 mutant with impaired caspase-3 association did not prevent telomere

damage–induced apoptosis, indicating that an association between p16 and caspase-3 proteins forces senescence induction by inhibiting caspase-3 activation and apoptosis. These results suggest that p16 plays a direct role in telomere damage–dependent senescence by limiting apoptosis via binding to caspase-3, revealing a direct link between telomere damage–dependent senescence and apoptosis with regards to aging and cancer.

## Introduction

Telomerase is composed of a catalytic reverse transcriptase (TERT) and telomeric template RNA (TR), which plays a key role in the elongation and maintenance of telomeres at chromosome ends (1-4). Shelterin complex proteins associate with telomere repeats for protection from inducing DNA damage response to overcome replicative end protection problem (5-8). Telomerase is highly expressed in stem cells, while it is inactivated due to epigenetic silencing of TERT upon differentiation in most somatic cell types (9,10). However, telomerase is reactivated in majority of cancer cells, inducing cell immortalization and tumorigenesis (11-14). Recent studies revealed a clinical relevance of TERT activation in cancer, as mutations within the core promoter region of the TERT gene provide binding sites for E-twenty-six (ETS) transcription factors, leading to cancer-specific telomerase reactivation (15-17).

Activation of telomerase protects cells from telomere damage, delaying senescence and

aging process (18,19), whereas targeting telomerase induces tumor suppressor responses such as senescence or apoptosis (20,21). However, signaling mechanisms that distinctly induce senescence versus apoptosis in non-cancerous versus cancerous cells in response to telomerase inactivation and telomere damage induction are largely unknown.

Sphingosine 1-phosphate (S1P) is a bioactive sphingolipid, generated by sphingosine kinase 1 or 2 (SPHK1 or SPHK2), that exerts pro-oncogenic signaling via engaging with its G-protein coupled receptors (S1PR1-5) in an autocrine or paracrine manner, and/or via directly binding to regulate its intracellular target proteins without receptor signaling (22-25). Intracellular targets of SPHK2-generated nuclear S1P include HDAC1/2 (26) and TERT (27). Our previous study described a role for SPHK2-generated S1P in the stabilization of telomerase via directly binding to hTERT involving its D684 residue (27). These studies also suggested that S1P binding mimicked the phosphorylation of hTERT at Ser<sup>921</sup>, which protected hTERT from ubiquitination and proteasomal degradation (27). However, roles and mechanisms by which targeting SPHK2/S1P and TERT induces senescence versus apoptosis with respect to telomere damage signaling and tumor suppression are largely unknown. Thus, in this study, we have outlined experiments to uncover signaling mechanisms that determine responses for the induction of senescence versus apoptosis via telomere damage-mediated cellular stress.

## Results

### Inhibition of SPHK2/S1P attenuates hTERT abundance and tumor growth

To determine the roles of SPHK2/S1P in the regulation of tumor suppression via controlling telomerase and telomere damage, we measured the effects of silencing and/or pharmacologic inhibition of SPHK2/S1P signaling using shRNA-dependent knockdown or small molecule inhibitor of SPHK2, ABC294640 (28-30) (Supplemental Fig. S1A) on the growth of A549 xenograft-derived tumors in SCID mice. ShRNA-mediated knockdown of SPHK2 (~75% mRNA reduction compared to Scr-shRNA-expressing tumors, measured by qPCR) almost completely prevented A549-xenograft-tumor growth compared to Scr-shRNA/A549-xenograft controls after 21 days

(Fig. 1A-B). Similarly, inhibition of SPHK2 using ABC294640 (100 mg/kg, 7 days/week treatment for 21 days) suppressed A549-xenograft-tumor growth compared to vehicle-treated controls (Fig. 1A). Interestingly, ABC294640 treatment had no additional effect on A549-xenograft-tumor growth suppression in response to shRNA-mediated SPHK2 knockdown, supporting its role in SPHK2 inhibition for tumor suppression (Fig. 1A). Suppression of A549-xenograft-tumor growth in response to SPHK2 knockdown or inhibition was consistent with decreased hTERT protein abundance and apoptosis measured by IHC using anti-hTERT antibody and TUNEL assay, respectively, compared to control tumor tissues (Fig. 1C-D). In addition, SPHK2 inhibition or knockdown resulted in increased telomere damage in A549-xenograft-tumors compared to controls, measured *ex vivo* by immunofluorescence using anti-TRF2 and anti- $\gamma$ -H2AX antibodies in TIF (telomere damage-induced foci) assay (31) (Fig. 1E). Moreover, there was no significant difference in the staining of senescence associated-beta galactosidase in shSPHK2 tumors compared to shScr controls (Fig. 1F). Similar data were also obtained when A549-luciferase derived tumors were grown orthotopically in the lungs of SCID mice after tail vein injection, and inhibition of SPHK2 using ABC294640 decreased lung tumor growth (~95%) and hTERT abundance compared to vehicle-treated controls (Supplemental Fig. S1B-D).

To assess the clinical relevance of hTERT regulation by SPHK2/S1P signaling, we then determined SPHK2 abundance with regard to hTERT expression by IHC using commercially available tumor microarrays (TMAs) containing lung tumor tissues obtained from patients with NSCLC (n=48) and their adjacent pathologically non-cancerous lung tissues (n=48). The data showed that SPHK2 is significantly over-expressed (~2.5-fold) in the majority of NSCLC tumors compared to their controls (46/48 tumors,  $p < 0.05$ ) (Supplemental Fig. S2A-B). The data also showed that hTERT was up-regulated (~2.8-fold) in the majority of NSCLC tumors (47/48,  $p < 0.05$ ) (Supplemental Fig. S2B). Importantly, the Spearman correlation analysis showed that there is a significant (n=48,  $p < 0.001$ ) association between SPHK2 and hTERT expression in these tissues (Supplemental Fig. S2C). Similar correlation

between SPHK2 and hTERT was detected in the majority of tumor tissues obtained from patients with small cell lung cancer (SCLC) (Supplemental Fig. S2D). Thus, these data suggest that targeting clinically relevant and upregulated SPHK2/S1P in tumors inhibits hTERT abundance, which is associated with increased telomere damage and apoptosis, leading to tumor growth suppression *in vivo*.

### **Targeting SPHK2/S1P signaling mediates telomere damage and subsequent caspase 3 activation in lung cancer and/or immortalized MEFs**

Because SPHK2 silencing or inhibition induced apoptosis (increased TUNEL staining) in ABC294640-derived lung tumor xenografts in SCID mice (Fig. 1D), we then measured the effects of ABC294640 on caspase activation using MEFs obtained from caspase3/caspase7 knockout mice (32), containing their various combinations of homozygous or heterozygous deletions. Treatment of caspase3<sup>+/-</sup>/caspase7<sup>+/-</sup> MEFs with ABC294640 (80  $\mu$ M, 8 h) increased caspase 3/7 activity ~2-fold compared to vehicle treated controls (Fig. 2A). Deletion of caspase 3 alone or in combination with caspase 7 completely abolished caspase activation in response to ABC294640 in caspase3<sup>-/-</sup>/caspase7<sup>+/-</sup> or caspase3<sup>+/-</sup>/caspase7<sup>-/-</sup> MEFs compared to controls (Fig. 2A). Interestingly, deletion of caspase 7 in caspase3<sup>+/-</sup>/caspase7<sup>-/-</sup> MEFs increased basal levels of caspase 3 activity compared to vehicle-treated caspase3<sup>+/-</sup>/caspase7<sup>+/-</sup> control MEFs, and ABC294640 was able to further induce caspase activity in caspase3<sup>+/-</sup>/caspase7<sup>-/-</sup> MEFs compared to their vehicle-treated controls. Moreover, ABC294640 increased telomere damage in a similar manner in caspase3<sup>+/-</sup>/caspase7<sup>+/-</sup> and caspase3<sup>-/-</sup>/caspase7<sup>+/-</sup> MEFs (Fig. 2B), suggesting that caspase 3 activation is regulated downstream of telomere damage in response to SPHK2 inhibition. These data were also consistent in A549 cells, in which ABC294640 induced caspase 3 activity ~1.8-fold compared to vehicle-treated controls, and inhibition of caspase 3 using Z-DEVD (33) pretreatment completely abrogated ABC294640-mediated caspase 3 activation (Fig. 2C). In reconstitution experiments in A549 cells stably expressing Scr or SPHK2 shRNAs, while ectopic expression of WT-SPHK2 protected caspase 3

activation in response to ABC294640, catalytically inactive mutant SPHK2<sup>G212E</sup> expression (34) was not protective compared to controls (Fig. 2D-E). Exogenous addition of S1P (5 $\mu$ M, 1h) also prevented ABC294640-mediated caspase 3 activation in A549 cells compared to vehicle-treated controls (Fig. 2F).

Increased telomere damage in response to genetic loss of SphK2 was also detected in SphK2<sup>-/-</sup> compared to WT-MEFs (Fig. 3A). Moreover, shRNA-mediated SPHK2 knockdown resulted in telomere damage in A549 cells compared to Scr-shRNA-transfected controls (Fig. 3B). As a control, we also detected the effects of hTERT knockdown on telomere damage in A549 cells in the absence/presence of ABC294640. ShRNA-mediated hTERT knockdown and SPHK2 inhibition using ABC294640 induced telomere damage at a similar level (~2.5-fold) compared to controls (Fig. 3C). However, inhibition of SPHK2 had no additional effect on telomere damage in response to hTERT knockdown (Fig. 3C). Moreover, shRNA-mediated knockdown of SphK2 or its pharmacologic inhibition using ABC294640 resulted in telomere damage and subsequent caspase 3 activation in A549 cells in response to G0/G1 arrest during serum starvation (Supplemental Fig. S3A-B and S3C-D). In addition, shRNA-mediated knockdown of SphK2 (Supplemental Fig. S4A) decreased S1P and dihydro-S1P without causing large changes in C16-ceramide or dihydro-C16-ceramide compared to Scr-shRNA-transfected cells (Supplemental Fig. S4B). These data suggest that telomere damage and/or caspase 3 activation in response to SphK2/S1P knockdown is regulated independently of cell cycle status and/or changes in ceramide and dihydro-ceramide accumulation in A549 cells.

However, SphK2 inhibition using ABC294640 mediated telomere damage without detectable caspase 3 activation in primary non-cancerous human lung fibroblasts (generation 2, Supplemental Fig. S5), suggesting that caspase 3 activation downstream of telomere damage might be regulated differentially in A549 lung cancer versus non-cancerous lung fibroblasts. Interestingly, inhibition of SPHK2/S1P signaling using ABC294640 had no effect on p53-induced DNA damage as measured by co-localization of p53 and  $\gamma$ -H2AX using immunofluorescence in A549 cells (Fig. 3D). Cisplatin exposure was used

as a positive control for p53-mediated DNA damage, which increased the co-localization of p53 and  $\gamma$ -H2AX in A549 cells compared to vehicle-treated controls (Fig. 3D). These data suggest that targeting SphK2/S1P signaling results in caspase 3 activation due to selective telomere damage, and not due to the activation of general DNA damage response.

### **SphK2/S1P inhibition leads to telomere damage through attenuation of S1P-hTERT association and phosphomimicking of telomerase**

To determine the involvement of hTERT in the regulation of telomere damage and subsequent caspase 3 activation, we performed studies in GM847 cells, which do not express endogenous TERT, but contain telomeric template RNA (27). In GM847 cells, ABC294640 increased caspase 3 activity ~3-fold compared to controls, and ectopic expression of WT-hTERT abrogated this ABC294640-mediated caspase activation (Fig. 4A-B). However, ectopic expression of a mutant hTERT with D684A conversion, with decreased S1P binding, was not protective for caspase 3 activation in response to ABC294640 (Fig. 4A-B). Moreover, expression of the phospho-mimic mutant of hTERT (S921D) with D684A conversion, which does not bind S1P (Supplemental Fig. S3C), was able to protect ABC294640-mediated caspase activation (Fig. 4A-B). Expression of WT- and mutant hTERT proteins was confirmed using Western blotting (Fig. 4D).

These data were also consistent with the effects of ectopic expression of WT-hTERT, but not D684A-hTERT with altered S1P binding, on the protection of telomere damage in response to SPHK2/S1P targeting using ABC294640 compared to vector-transfected controls (Fig. 5A-B). However, phospho-mimic mutant of hTERT restored telomere damage in response to ABC294640 even in the absence of S1P binding due to D684A conversion in cells that express D684A/S921D double mutation compared to controls, expressing S921A or S921D single mutations, which still bind S1P and protected telomere damage (Fig. 5A-B). Similarly, while ectopic expression of WT-hTERT prevented ABC294640-mediated cell death, measured by trypan blue exclusion assay, inhibition of S1P-hTERT binding by D684A mutation restored cell

death in response to ABC294640 compared to controls (Fig. 5C). However, phosphomimic S921D/D684A-hTERT mutant expression also prevented ABC294640-mediated cell death (Fig. 5C). Thus, these data suggest that S1P-binding to hTERT involving D684 protects telomere damage and caspase activation by mimicking phosphorylation of hTERT at Ser<sup>921</sup>. These data also suggest that targeting SPHK2/S1P signaling by ABC294640 induces telomere damage due to attenuation of S1P-hTERT association, leading to inhibition of phosphomimicking of hTERT, hTERT instability, and subsequent caspase 3 activation.

### **Activation of tumor suppressor TCF21 mediates telomere damage and caspase 3 activation in response to SphK2/S1P targeting**

To determine the signaling between SPHK2/S1P/hTERT targeting and caspase 3 activation, we measured the effects of SPHK2 knockdown on the expression of genes involved in lung tumor growth/suppression by q-PCR-based lung cancer specific RT<sup>2</sup> profiler PCR array (35) using total mRNA isolated from A549-xenograft-derived tumors expressing SPHK2 shRNA compared to Scr-shRNA expressing tumor controls (shown in Fig. 1A). The data showed that down-regulation of SPHK2 induced the expression of GPM6A, CA4, CDH13, TCF21, CDKN2A/OPCML and ERBB2 (~21-3-fold), while decreasing the expression of CXCL13, MMP9 and CLCA2 (~4-8-fold) compared to controls (Supplemental Fig. S6A). Among these, we were able to validate increased expression of tumor suppressor TCF21 (36) (~5-fold) in response to SPHK2 knockdown in A549 cells (Supplemental Fig. S6B). Moreover, shRNA-mediated knockdown of hTERT also induced TCF21 mRNA expression (~3.5-fold) compared to Scr-shRNA-expressing controls (Supplemental Fig. S6C). Ectopic expression of WT-hTERT, but not D684A-hTERT, prevented TCF21 mRNA induction in response to SPHK2 knockdown (Supplemental Fig. S6D). In addition, targeting SPHK2/S1P using ABC294640 induced TCF21 mRNA (~10-fold) and resulted in caspase 3 activation (~8-fold) compared to vehicle treated controls (Supplemental Fig. S4E-F). ShRNA-mediated knockdown of TCF21 (Supplemental Fig. S6E) prevented caspase 3 activation in

response to ABC294640 in A549 cells (Supplemental Fig. S6F).

To determine the effects of TCF21 activation in the regulation of lung tumor suppression in response to SPHK2/S1P/hTERT targeting *in vivo*, we measured the growth of A549-derived xenografts expressing Scr- or TCF21-shRNAs in the absence/presence of ABC294640. Treatment with ABC294640 (100 mg/kg at every 7 days for 21 days) inhibited the growth of Scr-shRNA expressing tumors compared to vehicle treated controls (Fig. 6A). ShRNA-mediated knockdown of TCF21 prevented ABC29464-mediated tumor suppression compared to controls (Fig. 6A). After growth measurements, remaining tumors were extracted from these mice, and effects of ABC294640 in the presence/absence of TCF21 knockdown on hTERT mRNA, caspase 3 activation and apoptosis were measured. ABC294640 reduced hTERT mRNA abundance in the presence/absence of TCF21 knockdown (Fig. 6B), suggesting that TCF21 induction is regulated downstream of hTERT down-regulation in response to targeting SPHK2/S1P signaling. Moreover, ABC294640 resulted in caspase 3 activation (measured by IHC) and apoptosis (measured by TEM), which were prevented in response to shRNA-mediated knockdown of TCF21 (Fig. 6C-D). ShRNA-mediated knockdown of TCF21 was confirmed in A549 xenograft-derived tumors *ex vivo* by qPCR (Fig. 6E). ShRNA-mediated knockdown of TCF21 had no detectable effects on telomere damage in response to ABC294640-mediated SPHK2 inhibition compared to control tumors (Fig. 6F-G). Thus, these data suggest a role for TCF21 induction in caspase 3 activation and apoptosis in response to the inhibition of SPHK2/S1P/hTERT axis and telomere damage by ABC294640, leading to tumor suppression.

### **Genetic loss of SphK2 results in accelerated senescence and aging via telomere damage and p16 induction without apoptosis in mice**

To determine the physiological impact of loss of SphK2/S1P signaling on senescence and aging due to TERT alterations in a non-cancerous model, we have generated subsequent generations of WT and SphK2<sup>-/-</sup> mice (for 6 generations). SphK2<sup>-/-</sup> mice exhibited accelerated senescence and aging phenotype measured by increased beta-

galactosidase expression in their paws (37) at generation 6, and decreased weight of testes at generation 4 or 5 compared to WT and SphK1<sup>-/-</sup> mice (generation matched controls) (Fig. 7A-B). Examining of spleen, skin and testes tissues at generation 6 using H&E staining also confirmed increased senescence and aging phenotype in SphK2<sup>-/-</sup> compared to WT mice.

SphK2<sup>-/-</sup> animals at generation 6 exhibited splenic atrophy with decreased white blood cells with no germinal centers present. It should be noted that the splenic atrophy is common in aged mice and can be accompanied with cachexia. There was decreased erythrocyte (red blood cell) turn over in the SphK2<sup>-/-</sup> mice, which might be due to decreased numbers of erythrocytes in circulation. Moreover, we observed decreased thickness of the hypodermal adipose layer in the SphK2<sup>-/-</sup> mice with multiple areas of inflammation, increased fibrosis and abnormal follicle development. Also, there were fewer seminiferous tubules (hypoplasia) in SphK2<sup>-/-</sup> mice compared to wild type control testes tissues (Fig. 7C).

In testes tissues, there was decreased mTERT abundance (measured by IHC) in SphK2<sup>-/-</sup> compared to WT and SphK1<sup>-/-</sup> mice (generation 6), whereas there was no apoptosis (measured by TUNEL staining) or TCF21 induction (measured by IHC) in these mice (Fig. 7D). In addition, telomere damage induction was detected in the testes of SphK2<sup>-/-</sup>, but not in WT or SphK1<sup>-/-</sup> mice (Fig. 7E). Thus, these data indicate that loss of SphK2 results in accelerated senescence and aging starting at generation 4, which is consistent with decreased mTERT and induction of telomere damage (especially in testes tissues). However, accelerated senescence/aging in mice appeared to be independent of TCF21 and/or apoptosis induction.

To further examine the effects of SphK2 loss, confirmed by Western blotting using anti-SphK2 antibody (38), in the induction of senescence, we have isolated MEFs at generations 4-6 from WT, SphK1<sup>-/-</sup> and SphK2<sup>-/-</sup> mice, and measured senescence by measuring b-gal and p16 expression. Induction of senescence was detected in the generation 4, 5 and 6 (G4-G6) of SphK2<sup>-/-</sup> compared to WT and SphK1<sup>-/-</sup> MEFs Fig. 8A-B). In addition, increased telomere damage was detected in SphK2<sup>-/-</sup> compared to WT and SphK1<sup>-/-</sup>

MEFs (Fig. 8C). Interestingly, while shRNA-mediated knockdown of p16 had no effect on telomere damage induction in SphK2<sup>-/-</sup> MEFs, it induced caspase 3 activation compared to controls (Fig. 8D). Collectively, these data suggest that loss of SphK2/S1P results in accelerated aging and senescence with p16 induction in SphK2<sup>-/-</sup> compared to WT and SphK1<sup>-/-</sup> mice at subsequent generations 4-6.

### **Induction of p16 distinctly mediates telomere-damage-mediated senescence and prevents apoptosis in response to SPHK2/S1P/telomerase targeting**

To determine whether alterations of SPHK2/S1P/hTERT signaling induces senescence in A549 lung cancer cells, which lack p16 expression (39), we measured the effects of down-regulation or inhibition of SPHK2 on caspase 3 activation and b-gal induction in the absence/presence of ectopic expression of p16. ShRNA-mediated knockdown of SPHK2 induced caspase 3 and ectopic expression of p16 attenuated this process compared to Scr-shRNA expressing A549 cells (Fig. 9A). ShRNA-dependent knockdown or ABC294640-mediated inhibition of SPHK2 had no detectable effect on the induction of senescence in A549 cells, whereas ectopic expression of p16 with/without SPHK2 targeting increased senescence in A549 cells compared to Scr-shRNA-expressing or vehicle-treated controls (Fig. 9B). Interestingly, while ectopic expression of p16 had no effect on the induction telomere damage (Fig. 9C), it completely prevented caspase 3 induction in response to SPHK2/S1P inhibition using ABC294640 compared to vehicle-treated controls (Fig. 9D-E). In reciprocal studies, shRNA-dependent knockdown of p16 in H1341 human lung cancer cells (confirmed by qPCR, Fig. 9F) resulted in enhanced caspase 3 activation in response to SPHK2 inhibition by ABC294640 compared to Scr-shRNA transfected controls (Fig. 9G). Lack of protein abundance of p16 in A549 and H157 human lung cancer cells compared to HeLa and H1341 cells, which express p16 is also confirmed by Western blotting (Fig. 9H). Thus, these data suggest that p16 expression determines the induction of senescence while inhibiting TCF21-dependent caspase 3 induction in response to

SPHK2/S1P/TERT targeting and telomere damage in lung cancer cells.

### **Interaction between p16 and caspase 3 prevents caspase 3 activation and apoptosis in response to telomere damage**

To define the mechanism by which p16 activation forces cell to undergo senescence but not apoptosis, we set out studies to test a novel hypothesis that interaction between p16 and caspase 3 might limit caspase 3 activation and prevent apoptosis. This hypothesis was first tested in H1341 human lung cancer cells, which express p16. SPHK2 inhibition by ABC294640 mediated the association between endogenous p16 and caspase 3 in H1341 cells, and this interaction was attenuated in response to shRNA-mediated silencing of p16 compared to controls (Fig. 10A). Similar data were also observed when SPHK2 expression was knocked down using shRNA, which resulted in increased association between ectopically expressed WT-p16 and caspase 3 in A549 cells with/without ABC294640 exposure compared to Scr-shRNA/vector-transfected and vehicle-treated controls using PLA and immunofluorescence (Fig. 10B-C). These data were also consistent when we measured the binding between recombinant and purified human p16 and caspase 3 proteins (40) using OpenSPR localized surface plasmon resonance (LSPR) biosensor at various protein concentrations. The data showed that purified p16 interacted with caspase 3 (KD, equilibrium dissociation constant=  $1.82 \times 10^{-8}$  +/-  $6.5 \times 10^{-9}$  M) (Supplemental Fig. S7A-B). Thus, these data suggest that p16 binding might prevent the activation of pro-caspase 3.

Next, using a molecular simulation and docking, we generated a model *in silico* for protein-protein interaction between p16 and caspase 3 using their existing structures determined by x-ray crystallography (Fig. 10D). The model suggested that the interaction between p16 and caspase 3 might involve Ser<sup>152</sup> of p16 (turquoise) and Gly<sup>251</sup> of caspase 3 (grey), which is within the activation domain of caspase 3 (His<sup>237</sup>-Cys<sup>285</sup>). To validate this model, we ectopically expressed WT-p16 and mutant-p16 with Ser<sup>152</sup> to Ala conversion, and measured their association in p16-null A549 cells using anti-p16 and anti-caspase 3 antibodies by PLA compared to vector-transfected controls. The data showed that

WT-p16 and caspase 3 association was induced in response to SPHK2 inhibition using ABC294640, whereas there was no detectable association between Ser<sup>152</sup>Ala-p16 in A549 cells (Fig. 10E). Moreover, ectopic expression of WT-p16 and not Ser<sup>152</sup>Ala-p16, largely protected cells from caspase 3 activation in response to ABC294640 exposure compared to vector-transfected controls (Fig 10F). Ectopic expression of WT-p16 and Ser<sup>152</sup>Ala-p16 in A549 cells was confirmed using Western blotting compared to vector-transfected controls using anti-p16 and anti-actin antibodies (Fig. 10G). Importantly, interaction between p16 and caspase 3 was also detected in testes tissues isolated from Sphk2-deficient mice at generation 5, which expressed SA- $\beta$ -Gal, but not in testes isolated from matched WT or SphK1<sup>-/-</sup> mice, which were also negative for SA- $\beta$ -Gal expression (Fig. 10H). Thus, these data suggest that interaction between p16 and caspase 3 involves the S152 residue of p16, and that this interaction is key to prevent caspase 3 activation, which forces senescence while limiting apoptotic cell death in response to SPHK2/S1P inhibition, and subsequent telomere damage.

## Discussion

Here, our data revealed that SPHK2-generated S1P binds and stabilizes TERT involving its D684 residue via mimicking TERT phosphorylation at S921, which protects telomere damage, and results in delayed senescence and protection from apoptosis. These data also suggested that targeting/inhibition of the SPHK2/S1P/telomerase axis results in telomere damage, which signals TCF21-dependent caspase 3 activation in cancer cells or immortalized MEFs, or p16-dependent senescence and accelerated aging phenotype in non-cancerous lung fibroblasts, primary MEFs (non-immortalized), and non-cancerous testes tissues in subsequent generations of SphK2<sup>-/-</sup> mice (Fig. 11). Mechanistically, this study demonstrated that interaction between p16 and caspase 3, involving Ser<sup>152</sup> of p16, prevents caspase 3 activation in response to telomere damage, forcing cells to selectively induce senescence but not apoptosis. Our previous study revealed that S1P-TERT binding, involving the D684 residue, stabilizes TERT via phosphomimic function of S1P at Ser<sup>921</sup> to regulate hTERT stability (27). Here, the data further suggested that while

targeting SPHK2/S1P induces hTERT degradation, resulting in telomere damage and apoptosis, expression of phosphomimic mutant of hTERT with S921D conversion even in the absence of S1P binding due to D684A mutation prevented telomere damage in response to SPHK2 inhibition. It will be interesting to define whether phosphomimic function of S1P upon binding to other proteins, such as HDAC1/2(26) and prohibitin 2 (41), or TRAF2 (22) and PPAR- $\gamma$  (42), play any roles in the regulation of their biological functions.

Interestingly, our current data also suggested that TCF21-dependent caspase 3 activation plays a key role in tumor suppression downstream of telomere damage in response to SPHK2/S1P targeting. TCF21 was reported as a tumor suppressor, whose expression is suppressed by epigenetic methylation in lung tumor tissues and cells (43,44). It was shown recently that TCF21 is reactivated by the expression of long noncoding RNA TARID, which enhanced its demethylation via GADD45A (45). It is, however, remains unknown whether SPHK2/S1P/TERT inhibition results in TCF21 activation through TARID/GADD45A.

In these studies, targeting SPHK2/S1P signaling using molecular (shRNA) or pharmacologic (ABC294640) tools resulted in consistent telomere damage in various cell types. Although ABC294640 is known to have off target effects, especially inducing the accumulation of dihydro-ceramides due to inhibition of DES (46,47), knocking down of SphK2 using shRNA had no effect on dihydro-ceramide accumulation (Supplemental Fig S4B). Thus, these data suggest that telomere damage evoked by SphK2 silencing or inhibition appears to be independent of ceramide/dihydro-ceramide alterations. However, effects of shRNA-mediated knockdown of SphK2 or its inhibition using ABC294640 on S1P versus ceramide and/or dihydroceramide accumulation in nuclear membranes need to be determined.

It was interesting that SphK2<sup>-/-</sup> mice showed accelerated telomere damage/senescence and aging phenotype after four generations. This was somewhat expected as mTERT<sup>-/-</sup> showed signs of telomere damage and aging phenotype after generation 4 also (48). Interestingly, while genetic loss of SphK2 induced senescence and aging due to telomerase instability and increased

telomere damage without induction of apoptosis in SphK2<sup>-/-</sup> compared to WT and SphK1<sup>-/-</sup> knockout mice, downregulation and/or inhibition of SPHK2/S1P/TERT signaling resulted in TCF21-dependent caspase 3 activation down stream of telomere damage in lung cancer cells. Our data further suggested that activation of p16 was the key to decide the fate of cells to succumb in senescence rather than apoptosis, as ectopic expression of p16 in p16-deficient cancer cells induced senescence by preventing caspase 3 activation. These data are consistent with a role of p16 in the protection of ATR4-mediated DNA damage in response to dysfunctional telomeres (49). Our data are also in agreement that in addition to p53 signaling, p16 is another effector protein for the telomere damage signaling (50). Moreover, recent studies suggest that p16-expressing cells shorten healthy life span (51), and that targeting p16 to clear senescent cells delays aging-related disorders detected in adipose tissue, skeletal muscle and eye (52), or rejuvenates aged hematopoietic stem cells in mice (53). These studies are consistent with our data, which provide a mechanistic link between p16 and inhibition of caspase 3 and apoptosis, supporting that targeting p16 induces clearance of senescent cells possibly by relieving caspase 3 from p16 for activation of caspase 3 and apoptosis. To this end, our data might have important clinical implications such that inhibition of p16 would switch senescent phenotype to apoptosis in tumors, improving tumor elimination and suppression, at least in part, in response to SPHK2/telomerase targeting.

Nevertheless, these data provide a novel link between the regulation of senescence versus caspase 3-dependent apoptosis, which is controlled by p16 signaling at least in response to telomere DNA damage evoked by SPHK2/S1P/TERT inhibition.

## Materials and Methods

### Cell lines and culture conditions

Cell lines were tested for mycoplasma contamination, and authenticated by short tandem repeat (STR) profiling (PowerPlex16HS) at the Genetica DNA Laboratories (Burlington, NC) in November 2016. A549 cells (expressing K-ras mutant, wild type p53) were grown in Dulbecco's Modified Eagle's Medium (DMEM) (Cellgro) with 10% fetal bovine serum (FBS) (Atlanta

Biologics) and 1% penicillin and streptomycin (Cellgro). H1299 (expressing wild type K-Ras, and lack expression of p53 due to a homozygous gene deletion) and H1341 cells were grown in RPMI-1640 (American type culture collection) with 10% fetal bovine serum and 1% penicillin and streptomycin. GM00847 cells were purchased from Coriell Cell Repositories. Wild type, SphK1<sup>-/-</sup>, SphK2<sup>-/-</sup> MEFs were obtained from K. Argraves (Medical University of South Carolina). GM00847 cells and MEFs were cultured in DMEM and incubated at 37°C with 5% CO<sub>2</sub>. Primary human lung fibroblasts were purchased from Lonza, Inc. and cultured in fibroblast growth media as described (27).

### Plasmids and shRNAs

Plasmid containing hTERT<sup>WT</sup> in pcDNA vector was obtained from J. Chen (Arizona State University) and site directed mutagenesis was performed to generate hTERT<sup>D684A</sup>, hTERT<sup>S921A</sup>, hTERT<sup>S921A-D684A</sup>, hTERT<sup>S921D</sup>, hTERT<sup>S921D-D684A</sup> using Q5 site directed mutagenesis kit (E0554S, New England Bio labs) using manufacturer's instructions. SPHK2<sup>WT</sup> and SPHK2<sup>G212E</sup> plasmids were obtained from Dr. Sarah Spiegel (Virginia Commonwealth University). pLenti-CMV p16-Neo(W111-1) (Plasmid# 22260) and pLenti-CMV Neo DEST (705-1) (Plasmid#17392) were obtained from Addgene. For knockdown studies, cells were plated at 40-50% confluency and Dharmafect transfection reagent I was used as per manufacturer's instructions. For SPHK2 knockdown, cells were transfected with 200nM siRNA (L-004831, Dharmacon, USA) for 72 h and for hTERT knockdown 100nM siRNA (L-003547, Dharmacon) was used.

SPHK2 shRNA (5'-3'):

CCGGCTACTTCTGCATCTACACCTACTCGA  
GTAGGTGTAGATGCAGAAGT-AGTTTTTTG  
(TRCN00000036973);

shTCF21#1(5'-3'):

CCGGCGTTTCCAAACCAGAGGAGATCTCG  
AGATCTCCTCTGGTTTGGAAACGTTTTT  
(TRCN0000015563);

shTCF21#2 (5'-3'):

CCGGCGACAAATACGAGAACGGGTACTCG  
AGTACCCGTTCTCGTATTTGTCGTTTTT  
(TRCN0000015563); and non-targeting shRNA

containing plasmids were purchased from Open Biosystems Inc. Plat-A or Plat-E cells were transfected using the viral transduction protocol as described by the RNA interference consortium (RNAi). The viral supernatants were added to either A549 cells or MEFs, and selection was performed using puromycin (1 µg/ml) for 14 days. The following shRNA's (Sigma) were obtained from MUSC shRNA shared technology resource :

sh-p16 (mouse) (5'-3'):  
CCGGGTGAACATGTTGTTGAGGCTACTCGA  
GTAGCCTCAACAACATGTTCACTTTTGG  
(TRCN0000077815);

sh-p16(Human) (5'-3'):  
CCGGCCGATTGAAAGAACCAGAGAGCTCG  
AGCTCTCTGGTCTTTCAATCGGTTTTG  
(TRCN0000265833)

### Visualization of S1P-hTERT or p16-caspase 3 interactions using proximity ligation assay (PLA)

GM00847 cells overexpressing hTERT<sup>S921D</sup>, hTERT<sup>S921D-D684A</sup> plasmids were fixed with 4% formalin for 15 minutes. Fixed and permeabilized cells were incubated with S1P specific antibody (Sphingomab, LT1002; 20 µg/ml) and hTERT antibody (ab32020, Abcam), or anti-p16 (A301-267A, Bethyl laboratories) and anti-caspase 3 (2305-PC-020, Trevigen) antibodies for 18 h. PLA was performed and visualized by IF-CM using Duolink in situ hybridization kit as described by the manufacturer (Olink Biosciences). Anti-IgG antibody was used as a negative control in PLA (27).

### Lung cancer specific Q-PCR based gene array

RT<sup>2</sup> profiler PCR array (PAHS-134C) from Qiagen was used for this purpose. Total RNA was isolated from shScr and shSPHK2 tumor tissues using RNeasy kit (Qiagen) with DNase digestion step and one µg of purified RNA was used for cDNA synthesis using iScript cDNA synthesis kit (Bio-Rad). PCR array was carried out using Applied Biosystems (ABI 7300) and analysis was performed as per manufacturer's instructions.

### Quantitative PCR (qPCR)

RNeasy (Qiagen) kit was used to isolate total RNA, and 1 µg of total RNA was used for

synthesizing complementary DNA (cDNA) using the iScript cDNA synthesis kit (Bio-Rad). Taqman probes (hTERT, Hs00162669\_m1; SPHK2, Hs00219999\_m1; TCF21, Hs00162646\_m1; *Tcf21*, Mm00448961\_m1; CDKN2A, Hs00923894\_m1; *Cdkn2a*, Mm00494449\_m1); Actb, Mm00607939\_s1; RPLPO, Hs99999902\_m1 were used for quantitative PCR (Life technologies).

### Antibodies

V5 (R960-25, Invitrogen), SPHK2 (1709-1AP, Proteintech and ab37977, Abcam),  $\gamma$ -H2AX (ab2893, Abcam), TRF-2 (IMG-124A, Imgenex), ki67 (ab15580, Abcam), p53 (#554294, BD Pharmingen), mTERT (sc-7212, Santa Cruz), hTERT (ab32020, Abcam), POD1 (mouse TCF21) (sc-7294, Santa Cruz), p16 (A301-267A, Bethyl laboratories), cleaved caspase-3 (2305-PC-020, Trevigen) antibodies were used.

### Immunohistochemistry and tumor micro array (TMA)

Lung adenocarcinoma TMA (LC1002) and Small cell lung cancer TMA (LC10010) was purchased from US Biomax and immunohistochemistry was performed with SPHK2 antibody (1:100) and hTERT antibody (1:50). Also, primary lung tumor tissues were obtained from the MUSC tumor biorepository core facility and immunohistochemistry was performed by fixing with formalin, embedding with paraffin and 5 µm sections were made for immunohistochemistry. Pathology analysis and scoring was performed by a pathologist at MUSC's biorepository core facility.

### Western blotting

1X10<sup>6</sup> A549 cells stably overexpressing either SPHK2<sup>WT</sup> or SPHK2<sup>G212E</sup> were plated in a 100mm petri dish overnight. The cells were harvested and centrifuged at 1300 rpm for 3.5 min and washed with 1X PBS (pH7.4) (Gibco). Cells were lysed with 1X CHAPS lysis buffer [10mM tris-HCl (pH7.5), 1mM MgCl<sub>2</sub>, 1mM EDTA, 0.1mM benzamidine, 5mM beta-mercaptoethanol, 0.5% CHAPS, 10% glycerol] including a protease inhibitor cocktail (Sigma-Aldrich) for 20 min on ice. Cell lysates were centrifuged at 12000g for 15 min at 4°C, and supernatants were used for Western Blotting. SDS-PAGE was carried out

using the Bio-Rad Criterion apparatus, followed by semi-dry transfer onto a polyvinylidene difluoride (PVDF) membrane. The membrane was blocked with 5% milk + 0.1% Tween-20 in 1X PBS (pH7.4). Primary antibodies were used at 1:1000 dilution overnight at 4°C, followed by rabbit or mouse secondary antibodies (Jackson Research Laboratories) conjugated with horseradish peroxidase at room temperature for 1 hour. The rabbit secondary antibody was used at 1:2500 for detecting hTERT and at 1: 5000 dilution for the rest of the antibodies. Actin was used as an internal control for Western blotting. The membranes were washed either with 1X PBS with Tween-20 or 1X tris-buffered saline with 0.1% Tween-20 and developed using ECL plus chemiluminescence detection kit (GE healthcare).

#### **Detection of telomere damage by TIF assay**

50,000 cells were plated in each of 4-well chamber slides overnight. Following treatment with ABC294640 (80  $\mu$ M for 8 hours), the cells were fixed in 4% paraformaldehyde in 1X PBS, pH7.4 for 15 minutes at room temperature. The slides were washed thrice with 1X PBS pH 7.4 and blocked with 1% goat serum in 0.3M glycine, 1% BSA and 0.1% Tween-20 in 1X PBS, pH7.4 for 2 hours. The cells were then incubated with primary antibodies that recognize  $\gamma$ -H2AX (5 $\mu$ g/ml; ab2893, Abcam) and TRF-2 (5 $\mu$ g/ml; IMG-124A, Imgenex) for 18 h. The slides were then washed thrice with 1X PBS, pH7.4 and incubated with secondary antibodies containing Alexa 488, Alexa 594 and Cy5 fluorophores against  $\gamma$ -H2AX and TRF-2, respectively for 2 h at 20-25 °C. The slides were then washed three times with 1X PBS, pH7.4 and DAPI containing mounting media was added and sealed with glass cover slips (colocalization resulted in either purple or yellow/orange images). Images were captured using IF-CM, and colocalization was quantified using Pearson's correlation coefficient was used to calculate colocalization efficiency and  $P < 0.05$  was considered significant by ImageJ Fiji software (27).

#### **Measurement of caspase 3 activation and apoptosis**

Active caspase-3 was measured using cleaved caspase-3 antibody (2305-PC-020) from Trevigen Inc. Immunofluorescence was performed using

Olympus FV10i microscope with 594- and 488-nm channels for visualizing red and green fluorescence. Images were taken at 60X magnification. At least three random fields were selected for images. Caspase-3/7 activity was measured in A549 cells and mouse embryonic fibroblasts by caspase-3 fluorometric assay kit (BF-1100, R&D systems) as per manufacturer instructions. Moreover, A549 cells were pretreated with Z-DEVD-FMK (caspase-3 specific inhibitor, FMK-004, R&D systems) at 10  $\mu$ M for two hours prior to ABC294640 treatment and caspase-3 activity measurement. Also, caspase-3 activity was measured using caspase-3 fluorometric kit following pretreatment with 5 $\mu$ M S1P. TUNEL assay: DeadEnd™ Colorimetric TUNEL System (G7360, Promega) was used for measuring TUNEL positive cells in mouse tissues as per manufacturer instructions.

#### **Serum starvation and cell cycle analysis by flow cytometry**

A549 cells ( $1 \times 10^6$ ) were seeded in 100 mm dishes and incubated at 37°C for 16 h before being switched to serum free media for 48 h. Then, cells were either treated with DMSO or 80  $\mu$ M ABC294640 for 8 additional hours. Cells were collected by trypsinization and washed twice in 1X PBS. The cells were then fixed for 30 minutes at 4°C in cold 70% ethanol (added drop-wise to the pellet while vortexing to ensure fixation of all cells and to minimize clumping). The pellets were spun at 850 g for 5 minutes, and rinsed twice with 1X PBS. The cells were then treated with ribonuclease, and 5  $\mu$ g/mL propidium iodide (PI) was added before analysis by FACS.

#### **Measurement of sphingolipids using mass spectrometry by lipidomics**

Sphingolipids in cells ( $1 \times 10^6$ ) were measured using mass spectrometry by lipidomics shared resource facility at the Medical University of South Carolina, as we described previously (54). The lipid abundance was normalized to inorganic phosphate (Pi),

#### **Ultra-structure analysis using TEM**

Formalin fixed shScr and shTCF21 tumors treated with ABC294640 or vehicle control were used. After post-fixation in 2% (v/v) osmium tetroxide, specimens were embedded in Epon 812, and

sections were cut orthogonally to the cell monolayer with a diamond knife. Thin sections were visualized in a JEOL 1010 TEM (55,56).

### **Detection of senescence**

A549 cancer cells and mouse embryonic fibroblasts (wild type, SphK1<sup>-/-</sup>, SphK2<sup>-/-</sup>) at passage 6 were plated in 60mm petri dishes for 18 hours followed by detection of senescence using senescence-associated  $\beta$ -galactosidase assay kit as described by the manufacturer (Cell Signaling Technology) (27).

### **Measurement of senescence, aging and tumor suppression in mice**

Mouse testes tissues at different mating generations and tumor xenografts were fresh frozen and 5 $\mu$ m tissue sections were cut and stained for senescence using senescence associated  $\beta$ -galactosidase assay kit as described by manufacturer's instructions (Cell Signaling Technology). SA- $\beta$ -galactosidase activity was also measured for paw tissues of mice from indicated genotypes using the same kit. All animal experiment protocols were approved by the Institutional Animal Care and Use Committee at the Medical University of South Carolina (27, 54-56).

### **Orthotopic lung tumor development in SCID mice**

SCID (severe combined immunodeficient) mice were purchased from Harlan laboratories. Age and sex matched mice (female SCID mice,  $n=7$ ) were used for this experiment. Mice were injected (100  $\mu$ l) with 1 million A549-Luciferase cells through tail vein and were allowed to colonize lungs. Ten days after tail vein injection, the mice were anesthetized with isoflurane and D-Luciferin was administered through intra peritoneal injection and luciferase bioluminescence was measured using Xenogen IVIS 200 Bioluminescence and Fluorescence Imaging System. Once luciferase expression was measured in the lungs of the animals they were segregated into two groups, one group received vehicle control (50%DMSO and 50% PEG-200) and the other received ABC294640 (100mg/Kg body weight) for 16 days. At the end of the experiment the mice were euthanized, lung tissues were collected and Ki-67

and hTERT levels were measured by immunohistochemistry.

### **Xenograft-derived tumors in SCID mice expressing stable shSPHK2**

A549 cells stably expressing SCR-shRNA or shRNA against SPHK2 (TRCN00000036973) were used for the experiment. Two million cells were implanted (100  $\mu$ l) into both flanks of SCID mice ( $n=4$  female SCID mice per group/ one tumor on each side of the flank) and when the tumors were palpable the mice were either treated with vehicle control or with ABC294640 at 100 mg/kg body weight for 21 days. Tumor volume was measured every alternative day using digital calipers and treatments were performed using oral gavage method every day. At the end of the experiment the mice were euthanized and tumor tissues were collected (27, 54-56).

### **Xenograft-derived tumors in SCID mice expressing stable shTCF21**

A549 cells stably expressing control shRNA or shRNA against TCF21 (TRCN0000015564, Open biosystems) were used for the experiment. Two million cells (100  $\mu$ l) were implanted into both flanks of female SCID mice ( $n=4$  mice per group/ one tumor on each side of the flank) and when the tumors were palpable the mice were either treated with vehicle control or with ABC294640 at 100 mg/kg body weight for 21 days. Tumor volume was measured every alternative day using digital calipers and treatments were performed using oral gavage method every day. At the end of the experiment the mice were euthanized and tumor tissues were collected (27, 54-57).

**Expression and purification of caspase 3.** Wild-type human caspase-3 was expressed in *E. coli* and purified using Ni-NTA agarose affinity resin, as described (58,59). Briefly, C-terminal His<sub>6</sub>-tagged plasmids pET23b-Casp3-His was purchased from Addgene (plasmid #'s 11821 and 90090, respectively) and transformed into *E. coli* strain C41(DE3). A single colony was used to inoculate 50 mL of LB containing 50  $\mu$ g/mL ampicillin and grown overnight at 37 °C. This culture was diluted 1:2000 into 4x250 mL of LB media and incubated at 37 °C until the OD<sub>600</sub> reached 3-5. Rich media was exchanged to a minimal formulation suitable for high-density

IPTG induction by spinning the cells gently at 5,000 x g for 10 min at 20-25 °C, and then resuspending in an equal volume of minimal media. Cultures were incubated at 37 °C until the OD<sub>600</sub> increased by at least 1 unit, the incubator was lowered to 18 °C, and protein expression was induced with 1 mM IPTG for 16 h at 170 rpm. The cells were pelleted at 10,000 x g for 20 min and were resuspended in lysis/binding buffer A (20mM HEPES pH 7.5, 1M NaCl, 20 mM imidazole and 10 mM β-mercaptoethanol). Following sonication and centrifugation at 18,000 x g for 30 min, the cleared lysate was applied to an equilibrated 1 ml HisTrap FF column (GE Healthcare, catalog No. 17-5255-01), washed with 10 column volumes of wash buffer (10% Buffer B; 20mM HEPES pH 7.5, 1M NaCl, 250 mM imidazole and 10 mM β-mercaptoethanol) and eluted by a linear gradient of imidazole from 10-70% over 40 column volumes using an ÄKTA start FPLC (GE Healthcare Life Sciences). The eluted fractions were analyzed by SDS-PAGE and fractions containing caspase-3 were supplemented with 5 mM TCEP, concentrated to 2 mL and applied to a HiPrep™ 16/60 Sephacryl™ S-200 HR size exclusion column in SEC Buffer C (50 mM HEPES pH 7.5, 300 mM NaCl, 10 mM β-mercaptoethanol 1 mM EDTA, and 10% glycerol). Fractions containing pure caspase-3 as determined by 4-20% SDS-PAGE were pooled, quantified, and stored at -80 °C as 1 mL aliquots.

### **Molecular modeling and OpenSPR for measurements of protein-protein interactions**

The existing PDB files containing NMR structure of p16 (2A5E) and X-ray crystallography structure of caspase 3 (5IBP) from RSCB ([www.rscb.org](http://www.rscb.org)) were transferred into ZDOCK Server (<http://zdock.umassmed.edu/>). The top model was then used to predict the sites of association between p16 and caspase 3, as we described (57).

The protein-protein association between recombinant purified human p16 (Novus Biologicals, NBP2-35199) and caspase 3 was measured using an OpenSPR localized surface plasmon resonance (LSPR) biosensor (Nicoya Life Science, Inc., Kitchener, Canada), as described previously (60). In short, 100 μL (50 μg/ml) of p16<sup>Ink4a</sup>, purchased from Novus Biologicals (#NBP2-35199), was immobilized on a COOH sensor chip (Nicoya # SEN-AU-100-12-COOH) at

a flow rate of 20 μL/min in 1X PBS buffer (pH 7.4) and 0.1% v/v Tween 20. Free activated carboxyl groups were deactivated with the addition of 100 μL blocking buffer (Nicoya). The immobilized ligand was washed with analyte running buffer (1X PBS, pH 7.4; 0.1% v/v Tween 20; 0.1% w/v BSA) until a stable baseline was achieved. Buffer-matched recombinant caspase 3 (80 μL; 50-1000 nM) analytes were injected into the flow cell at a rate of 20 μL/min. Following a 4-minute interaction time, the dissociation was recorded for an additional 16 minutes. The ligand-immobilized sensor chip was regenerated between each analyte injection using 20 mM HCl at a 150 μL/min flow rate. Kinetic binding analysis was performed with the TraceDrawer software package (Ridgeview Instruments, Uppsala, Sweden). Sensorgram traces were fit to a 1:1 Langmuir model to derive association (K<sub>a</sub>), dissociation (K<sub>d</sub>), and affinity (K<sub>D</sub>) constants.

### **Statistical Analyses**

All data are presented as mean ± SD, and group comparisons were performed with a two-tailed Student's *t* test. Wilcoxon rank sum test and paired *t*-test were used to analyze small-cell and non-small cell tumor microarray data. Tumor xenograft experiments were analyzed using two-way ANOVA with Tukey's posthoc test and testes weights from G4 and G5 mice were analyzed using one-way ANOVA with Tukey's posthoc test. The results were analysed using GraphPad Prism 7 software and *P*<0.05 was considered statistically significant (27, 54-56). For the comparison of several groups, a variance analysis (ANOVA) was carried out under normal distribution assumption.

### **Acknowledgements**

We thank Dr. Richard Flavell (Yale University) for providing us with the caspase3/7 knockout MEFs. We thank Dr. Sarah Spiegel (Virginia Commonwealth University) for providing SphK2 plasmids. The authors also thank Dr. Elizabeth Garrett-Mayer (MUSC) for her assistance with statistical analyses and discussions in this study. This work is supported by research funding from the National Institutes of Health (R01-CA088932, R01-CA173687, R01-DE016572, and P01-CA203628 to BO). The core facilities utilized were constructed using support from NIH (C06

RR015455), Hollings Cancer Center Support Grant (P30 CA138313), or Center of Biomedical Research Excellence (Cobre) in Lipidomics and Pathobiology (P30 GM103339).

### Conflict of Interest Statement

The authors declare no conflict of interest.

### Author Contributions

S.P.S. designed and performed experiments, analyzed data, prepared the figures, and helped write the manuscript; M.C. designed animal breedings and prepared tissue sections from mice; K.H. prepared tissues from mice and provided pathological analyses of the tissue slides; C.D.S. synthesized and provided ABC294640; B.O. designed experiments, analyzed data, and wrote the manuscript.

### For more information

Lipidomics:

<http://www.hollingscancercenter.org/research/shared-resources/lipidomics/index.html>

### References

1. Cohen, S. B., Graham, M. E., Lovrecz, G. O., Bache, N., Robinson, P. J., and Reddel, R. R. (2007) Protein composition of catalytically active human telomerase from immortal cells. *Science* **315**, 1850-1853
2. Gillis, A. J., Schuller, A. P., and Skordalakes, E. (2008) Structure of the *Tribolium castaneum* telomerase catalytic subunit TERT. *Nature* **455**, 633-637
3. Greider, C. W., and Blackburn, E. H. (1987) The telomere terminal transferase of *Tetrahymena* is a ribonucleoprotein enzyme with two kinds of primer specificity. *Cell* **51**, 887-898
4. Jiang, J., Chan, H., Cash, D. D., Miracco, E. J., Ogorzalek Loo, R. R., Upton, H. E., Cascio, D., O'Brien Johnson, R., Collins, K., Loo, J. A., Zhou, Z. H., and Feigon, J. (2015) Structure of *Tetrahymena* telomerase reveals previously unknown subunits, functions, and interactions. *Science* **350**, aab4070
5. Doksani, Y., Wu, J. Y., de Lange, T., and Zhuang, X. (2013) Super-resolution fluorescence imaging of telomeres reveals TRF2-dependent T-loop formation. *Cell* **155**, 345-356
6. Timashev, L. A., Babcock, H., Zhuang, X., and de Lange, T. (2017) The DDR at telomeres lacking intact shelterin does not require substantial chromatin decompaction. *Genes Dev* **31**, 578-589
7. de Lange, T. (2005) Shelterin: the protein complex that shapes and safeguards human telomeres. *Genes Dev* **19**, 2100-2110
8. Rice, C., Shastrula, P. K., Kossenkov, A. V., Hills, R., Baird, D. M., Showe, L. C., Doukov, T., Janicki, S., and Skordalakes, E. (2017) Structural and functional analysis of the human POT1-TPP1 telomeric complex. *Nat Commun* **8**, 14928
9. Counter, C. M., Hahn, W. C., Wei, W., Caddle, S. D., Beijersbergen, R. L., Lansdorp, P. M., Sedivy, J. M., and Weinberg, R. A. (1998) Dissociation among in vitro telomerase activity, telomere maintenance, and cellular immortalization. *Proc Natl Acad Sci U S A* **95**, 14723-14728
10. Gunes, C., and Rudolph, K. L. (2013) The role of telomeres in stem cells and cancer. *Cell* **152**, 390-393
11. Valentijn, L. J., Koster, J., Zwijnenburg, D. A., Hasselt, N. E., van Sluis, P., Volckmann, R., van Noesel, M. M., George, R. E., Tytgat, G. A., Molenaar, J. J., and Versteeg, R. (2015) TERT rearrangements are frequent in neuroblastoma and identify aggressive tumors. *Nat Genet* **47**, 1411-1414
12. Hahn, W. C., Stewart, S. A., Brooks, M. W., York, S. G., Eaton, E., Kurachi, A., Beijersbergen, R. L., Knoll, J. H., Meyerson, M., and Weinberg, R. A. (1999) Inhibition of telomerase limits the growth of human cancer cells. *Nat Med* **5**, 1164-1170
13. Bodnar, A. G., Ouellette, M., Frolkis, M., Holt, S. E., Chiu, C. P., Morin, G. B., Harley, C. B., Shay, J. W., Lichtsteiner, S., and Wright, W. E. (1998) Extension of life-span by introduction of telomerase into normal human cells. *Science* **279**, 349-352

14. Walsh, K. M., Codd, V., Smirnov, I. V., Rice, T., Decker, P. A., Hansen, H. M., Kollmeyer, T., Kosel, M. L., Molinaro, A. M., McCoy, L. S., Bracci, P. M., Cabriga, B. S., Pekmezci, M., Zheng, S., Wiemels, J. L., Pico, A. R., Tihan, T., Berger, M. S., Chang, S. M., Prados, M. D., Lachance, D. H., O'Neill, B. P., Sicotte, H., Eckel-Passow, J. E., Group, E. C. T., van der Harst, P., Wiencke, J. K., Samani, N. J., Jenkins, R. B., and Wrensch, M. R. (2014) Variants near TERT and TERC influencing telomere length are associated with high-grade glioma risk. *Nat Genet* **46**, 731-735
15. Horn, S., Figl, A., Rachakonda, P. S., Fischer, C., Sucker, A., Gast, A., Kadel, S., Moll, I., Nagore, E., Hemminki, K., Schadendorf, D., and Kumar, R. (2013) TERT promoter mutations in familial and sporadic melanoma. *Science* **339**, 959-961
16. Li, Y., Zhou, Q. L., Sun, W., Chandrasekharan, P., Cheng, H. S., Ying, Z., Lakshmanan, M., Raju, A., Tenen, D. G., Cheng, S. Y., Chuang, K. H., Li, J., Prabhakar, S., Li, M., and Tergaonkar, V. (2015) Non-canonical NF-kappaB signalling and ETS1/2 cooperatively drive C250T mutant TERT promoter activation. *Nat Cell Biol* **17**, 1327-1338
17. Huang, F. W., Hodis, E., Xu, M. J., Kryukov, G. V., Chin, L., and Garraway, L. A. (2013) Highly recurrent TERT promoter mutations in human melanoma. *Science* **339**, 957-959
18. Vega, L. R., Mateyak, M. K., and Zakian, V. A. (2003) Getting to the end: telomerase access in yeast and humans. *Nat Rev Mol Cell Biol* **4**, 948-959
19. Montero, J. J., Lopez de Silanes, I., Grana, O., and Blasco, M. A. (2016) Telomeric RNAs are essential to maintain telomeres. *Nat Commun* **7**, 12534
20. Shay, J. W. (2016) Role of Telomeres and Telomerase in Aging and Cancer. *Cancer Discov* **6**, 584-593
21. Balk, B., Maicher, A., Dees, M., Klermund, J., Luke-Glaser, S., Bender, K., and Luke, B. (2013) Telomeric RNA-DNA hybrids affect telomere-length dynamics and senescence. *Nat Struct Mol Biol* **20**, 1199-1205
22. Alvarez, S. E., Harikumar, K. B., Hait, N. C., Allegood, J., Strub, G. M., Kim, E. Y., Maceyka, M., Jiang, H., Luo, C., Kordula, T., Milstien, S., and Spiegel, S. (2010) Sphingosine-1-phosphate is a missing cofactor for the E3 ubiquitin ligase TRAF2. *Nature* **465**, 1084-1088
23. Hannun, Y. A., and Obeid, L. M. (2008) Principles of bioactive lipid signalling: lessons from sphingolipids. *Nat Rev Mol Cell Biol* **9**, 139-150
24. Ogretmen, B. (2018) Sphingolipid metabolism in cancer signalling and therapy. *Nat Rev Cancer* **18**, 33-50
25. Pyne, N. J., and Pyne, S. (2010) Sphingosine 1-phosphate and cancer. *Nat Rev Cancer* **10**, 489-503
26. Hait, N. C., Allegood, J., Maceyka, M., Strub, G. M., Harikumar, K. B., Singh, S. K., Luo, C., Marmorstein, R., Kordula, T., Milstien, S., and Spiegel, S. (2009) Regulation of histone acetylation in the nucleus by sphingosine-1-phosphate. *Science* **325**, 1254-1257
27. Panneer Selvam, S., De Palma, R. M., Oaks, J. J., Oleinik, N., Peterson, Y. K., Stahelin, R. V., Skordalakes, E., Ponnusamy, S., Garrett-Mayer, E., Smith, C. D., and Ogretmen, B. (2015) Binding of the sphingolipid S1P to hTERT stabilizes telomerase at the nuclear periphery by allosterically mimicking protein phosphorylation. *Sci Signal* **8**, ra58
28. Lewis, C.S., Voelkel-Johnson, C., and Smith, C.D (2016). Suppression of c-Myc and RRM2 expression in pancreatic cancer cells by the sphingosine kinase-2 inhibitor ABC294640. *Oncotarget* **7**, 60181-60192
29. French, K. J., Zhuang, Y., Maines, L. W., Gao, P., Wang, W., Beljanski, V., Upson, J. J., Green, C. L., Keller, S. N., and Smith, C. D. (2010) Pharmacology and antitumor activity of ABC294640, a selective inhibitor of sphingosine kinase-2. *J Pharmacol Exp Ther* **333**, 129-139
30. Venkata, J. K., An, N., Stuart, R., Costa, L. J., Cai, H., Coker, W., Song, J. H., Gibbs, K., Matson, T., Garrett-Mayer, E.,

- Wan, Z., Ogretmen, B., Smith, C., and Kang, Y. (2014) Inhibition of sphingosine kinase 2 downregulates the expression of c-Myc and Mcl-1 and induces apoptosis in multiple myeloma. *Blood* **124**, 1915-1925
31. Mender, I., and Shay, J. W. (2015) Telomere Dysfunction Induced Foci (TIF) Analysis. *Bio Protoc* **5**
32. Lakhani, S. A., Masud, A., Kuida, K., Porter, G. A., Jr., Booth, C. J., Mehal, W. Z., Inayat, I., and Flavell, R. A. (2006) Caspases 3 and 7: key mediators of mitochondrial events of apoptosis. *Science* **311**, 847-851
33. Igarashi, N., Okada, T., Hayashi, S., Fujita, T., Jahangeer, S., and Nakamura, S. (2003) Sphingosine kinase 2 is a nuclear protein and inhibits DNA synthesis. *J Biol Chem* **278**, 46832-46839
34. Hait, N. C., Bellamy, A., Milstien, S., Kordula, T., and Spiegel, S. (2007) Sphingosine kinase type 2 activation by ERK-mediated phosphorylation. *J Biol Chem* **282**, 12058-12065
35. Ponnusamy, S., Selvam, S. P., Mehrotra, S., Kawamori, T., Snider, A. J., Obeid, L. M., Shao, Y., Sabbadini, R., and Ogretmen, B. (2012) Communication between host organism and cancer cells is transduced by systemic sphingosine kinase 1/sphingosine 1-phosphate signalling to regulate tumour metastasis. *EMBO Mol Med* **4**, 761-775
36. Smith, L. T., Lin, M., Brena, R. M., Lang, J. C., Schuller, D. E., Otterson, G. A., Morrison, C. D., Smiraglia, D. J., and Plass, C. (2006) Epigenetic regulation of the tumor suppressor gene TCF21 on 6q23-q24 in lung and head and neck cancer. *Proc Natl Acad Sci U S A* **103**, 982-987
37. Pont, A. R., Sadri, N., Hsiao, S. J., Smith, S., and Schneider, R. J. (2012) mRNA decay factor AUF1 maintains normal aging, telomere maintenance, and suppression of senescence by activation of telomerase transcription. *Mol Cell* **47**, 5-15
38. Neubauer, H. A., and Pitson, S. M. (2016) Validation of commercially available sphingosine kinase 2 antibodies for use in immunoblotting, immunoprecipitation and immunofluorescence. *F1000Res* **5**, 2825
39. Masterson, J. C., and O'Dea, S. (2007) 5-Bromo-2-deoxyuridine activates DNA damage signalling responses and induces a senescence-like phenotype in p16-null lung cancer cells. *Anticancer Drugs* **18**, 1053-1068
40. Bose, K., Pop, C., Feeney, B., and Clark, A.C. (2003) An uncleavable procaspase-3 mutant has a lower catalytic efficiency but an active site similar to that of mature caspase-3. *Biochemistry* **42**, 12298-12310
41. Strub, G. M., Paillard, M., Liang, J., Gomez, L., Allegood, J. C., Hait, N. C., Maceyka, M., Price, M. M., Chen, Q., Simpson, D. C., Kordula, T., Milstien, S., Lesnefsky, E. J., and Spiegel, S. (2011) Sphingosine-1-phosphate produced by sphingosine kinase 2 in mitochondria interacts with prohibitin 2 to regulate complex IV assembly and respiration. *FASEB J* **25**, 600-612
42. Parham, K. A., Zebol, J. R., Tooley, K. L., Sun, W. Y., Moldenhauer, L. M., Cockshell, M. P., Gliddon, B. L., Moretti, P. A., Tigyi, G., Pitson, S. M., and Bonder, C. S. (2015) Sphingosine 1-phosphate is a ligand for peroxisome proliferator-activated receptor-gamma that regulates neoangiogenesis. *FASEB J* **29**, 3638-3653
43. Richards, K. L., Zhang, B., Sun, M., Dong, W., Churchill, J., Bachinski, L. L., Wilson, C. D., Baggerly, K. A., Yin, G., Hayes, D. N., Wistuba, II, and Krahe, R. (2011) Methylation of the candidate biomarker TCF21 is very frequent across a spectrum of early-stage nonsmall cell lung cancers. *Cancer* **117**, 606-617
44. Tessema, M., Willink, R., Do, K., Yu, Y. Y., Yu, W., Machida, E. O., Brock, M., Van Neste, L., Stidley, C. A., Baylin, S. B., and Belinsky, S. A. (2008) Promoter methylation of genes in and around the

- candidate lung cancer susceptibility locus 6q23-25. *Cancer Res* **68**, 1707-1714
45. Arab, K., Park, Y. J., Lindroth, A. M., Schafer, A., Oakes, C., Weichenhan, D., Lukanova, A., Lundin, E., Risch, A., Meister, M., Dienemann, H., Dyckhoff, G., Herold-Mende, C., Grummt, I., Niehrs, C., and Plass, C. (2014) Long noncoding RNA TARID directs demethylation and activation of the tumor suppressor TCF21 via GADD45A. *Mol Cell* **55**, 604-614
  46. Venant, H., Rahmaniyan, M., Jones, E.E., Lu, P., Lilly, M.B., Garrett-Mayer, E., Drake, R.R., Kravetska, J.M., Smith, C.D., and Voelkel-Johnson, C. (2015) The sphingosine kinase 2 inhibitor ABC294640 reduces the growth of prostate cancer cells and results in accumulation of dihydroceramides in vitro and in vivo. *Mol Cancer Ther.* **14**, 2744-2752
  47. Britten, C.D., Garrett-Mayer, E., Chin, S.H., Shirai, K., Ogretmen, B., Bentz, T.A., Brisendine, A., Anderton, K., Cusack, S.L., Maines, L.W., Zhuang, Y., Smith, C.D., and Thomas, M.B. (2017) A Phase I study of ABC294640, a first-in-class sphingosine kinase-2 inhibitor, in patients with advanced solid tumors. *Clin Cancer Res.* **23**, 4642-4650
  48. Blasco, M. A., Lee, H. W., Hande, M. P., Samper, E., Lansdorp, P. M., DePinho, R. A., and Greider, C. W. (1997) Telomere shortening and tumor formation by mouse cells lacking telomerase RNA. *Cell* **91**, 25-34
  49. Wang, Y., Sharpless, N., and Chang, S. (2013) p16(INK4a) protects against dysfunctional telomere-induced ATR-dependent DNA damage responses. *J Clin Invest* **123**, 4489-4501
  50. Jacobs, J. J., and de Lange, T. (2005) p16INK4a as a second effector of the telomere damage pathway. *Cell Cycle* **4**, 1364-1368
  51. Baker, D. J., Childs, B. G., Durik, M., Wijers, M. E., Sieben, C. J., Zhong, J., Saltness, R. A., Jeganathan, K. B., Verzosa, G. C., Pezeshki, A., Khazaie, K., Miller, J. D., and van Deursen, J. M. (2016) Naturally occurring p16(Ink4a)-positive cells shorten healthy lifespan. *Nature* **530**, 184-189
  52. Baker, D. J., Wijshake, T., Tchkonja, T., LeBrasseur, N. K., Childs, B. G., van de Sluis, B., Kirkland, J. L., and van Deursen, J. M. (2011) Clearance of p16Ink4a-positive senescent cells delays ageing-associated disorders. *Nature* **479**, 232-236
  53. Chang, J., Wang, Y., Shao, L., Laberge, R. M., Demaria, M., Campisi, J., Janakiraman, K., Sharpless, N. E., Ding, S., Feng, W., Luo, Y., Wang, X., Aykin-Burns, N., Krager, K., Ponnappan, U., Hauer-Jensen, M., Meng, A., and Zhou, D. (2016) Clearance of senescent cells by ABT263 rejuvenates aged hematopoietic stem cells in mice. *Nat Med* **22**, 78-83
  54. Gencer, S., Oleinik, N., Kim, J., Panneer Selvam, S., De Palma, R., Dany, M., Nganga, R., Thomas, R.J., Senkal, C.E., Howe, P.H., and Ogretmen, B. (2017) TGF- $\beta$  receptor I/II trafficking and signaling at primary cilia are inhibited by ceramide to attenuate cell migration and tumor metastasis. *Sci Signal.* **10**. pii: eaam7464
  55. Dany, M., Gencer, S., Nganga, R., Thomas, R. J., Oleinik, N., Baron, K. D., Szulc, Z. M., Ruvolo, P., Kornblau, S., Andreeff, M., and Ogretmen, B. (2016) Targeting FLT3-ITD signaling mediates ceramide-dependent mitophagy and attenuates drug resistance in AML. *Blood* **128**, 1944-1958
  56. Sentelle, R. D., Senkal, C. E., Jiang, W., Ponnusamy, S., Gencer, S., Selvam, S. P., Ramshesh, V. K., Peterson, Y. K., Lemasters, J. J., Szulc, Z. M., Bielawski, J., and Ogretmen, B. (2012) Ceramide targets autophagosomes to mitochondria and induces lethal mitophagy. *Nat Chem Biol* **8**, 831-838
  57. Thomas, R. J., Oleinik, N., Panneer Selvam, S., Vaena, S. G., Dany, M., Nganga, R. N., Depalma, R., Baron, K. D.,

- Kim, J., Szulc, Z. M., and Ogretmen, B. (2017) HPV/E7 induces chemotherapy-mediated tumor suppression by ceramide-dependent mitophagy. *EMBO Mol Med* **9**, 1030-1051
58. Hwang, D., Kim, S.A., Yang, E.G., Song, H.K., and Chung, H.S. A facile method to prepare large quantities of active caspase-3 overexpressed by auto-induction in the C41(DE3) strain. (2016) *Protein Expr Purif* **126**, 104–108
59. Sivashanmugam, A., Murray, V., Cui, C., Zhang, Y., Wang, J., and Li, Q. Practical protocols for production of very high yields of recombinant proteins using *Escherichia coli*. (2009) *Protein Sci* **18**, 936–948
60. McGurn, L.D., Moazami-Goudarzi, M., White, S.A., Suwal, T., Brar, B., Tang, J.Q., Espie, G.S., and Kimber, M.S. (2016) The structure, kinetics and interactions of the  $\beta$ -carboxysomal  $\beta$ -carbonic anhydrase, CcaA. *Biochem J* **473**, 4559-4572

## Figure Legends

**Fig. 1. Inhibition of SphK2 attenuates tumor growth in vivo.** (A) Effects of shRNA-dependent silencing of SPHK2 on A549 xenograft-derived tumor growth in the presence/absence of ABC294640 (n=4 mice per group, each containing two tumors on both flanks) were measured in SCID mice for 21 days (upper panel). Tumor growth was measured every alternative day for upto 21 days by calipers. After the growth study was completed, the tumors were removed and measured *ex vivo* (lower panel). Two way ANOVA with Tukey's posthoc test was performed. shScr Vs ShScr+ABC(\* $P$ <0.001,  $F$ =22.76,  $DF$ =27), shScr Vs shSK2(\*\* $P$ <0.001,  $F$ =35.48,  $DF$ =9), shSK2 versus shSK2 + ABC(\*\* $P$ =0.997). (B) ShRNA-mediated knockdown of ISPHK2 mRNA in A549 xenograft-derived tumors was confirmed using qPCR after the tumor growth measurements were completed. Data are means  $\pm$  SD from three independent experiments, analysed by student's t-test (n=3, \* $P$ =0.039, \*\* $P$ =0.014). (C-D) Effects of shRNA-mediated knockdown and/or ABC294640-dependent inhibition of SPHK2 on hTERT expression (C) or apoptosis (D) measured using IHC or TUNEL staining (Data are means  $\pm$  SD from three

independent experiments, analysed by student's t-test, n=3, \* $P$ =0.025, \*\* $P$ =0.042, \*\*\* $P$ =0.66), respectively, were measured in A549 xenograft-derived tumors. Scale bars represent 100  $\mu$ m. (E-F) Telomere damage (E) in A549 xenograft-derived tumors expressing Scr- or SPHK2-shRNAs in the absence/presence of ABC294640 were measured using TIF assay. Quantification of images were performed using Image J (right panel). Data are means  $\pm$  SD from three independent experiments, analysed by student's t-test (n=3, \* $P$ =0.006, \*\* $P$ =0.013, \*\*\* $P$ =0.003). (F) Senescence in A549 derived tumors expressing Scr-or SPHK2-shRNAs in the absence/presence of ABC294640 were measured using SA-beta-gal staining. Scale bars represent 100  $\mu$ m.

**Fig. 2. SphK2 targeting using ABC294640 induces caspase 3-dependent apoptosis.** (A) Effects of ABC294640 on apoptosis induction were measured in immortalized MEFs isolated from Casp3<sup>+/-</sup>/Casp7<sup>+/-</sup>, Casp3<sup>-/-</sup>/Casp7<sup>+/-</sup>, Casp3<sup>+/-</sup>/Casp7<sup>-/-</sup>, and Casp3<sup>-/-</sup>/Casp7<sup>-/-</sup> mice were measured compared to vehicle-treated controls using caspase 3/7 activity assay compared to vehicle-treated controls. Data are means  $\pm$  SD from three independent experiments, analysed by student's t-test (n=3, \* $P$ =0.006, \*\* $P$ =0.013, \*\*\* $P$ =0.003, \*\*\*\* $P$ =0.003). (B) Telomere damage in response to ABC294640-mediated SphK2 inhibition was measured in MEFs isolated from WT and Casp3<sup>-/-</sup>/Casp7<sup>+/-</sup> mice using TIF assay. Quantification of images were performed using Image J (right panel). Data are means  $\pm$  SD from three independent experiments, analysed by student's t-test (n=3, \* $P$ =0.03, \*\* $P$ =0.042). Scale bars represent 100  $\mu$ m. (C) Effects of caspase 3 inhibition using Z-DEVD on apoptosis in response to SPHK2 inhibition by ABC294640 were measured using caspase 3/7 activity assay in A549 cells compared to vehicle-treated controls. Data are means  $\pm$  SD from three independent experiments, analysed by student's t-test (n=3, \* $P$ =0.042, \*\* $P$ =0.033). (D) Ectopic expression of WT-SphK2-V5 and SphK2<sup>G212E</sup>-V5 compared to empty vector-V5 in A549 cells transfected with Scr- or SphK2-shRNAs were confirmed by Western blotting using anti-V5 antibody (upper panel). Actin was measured as a loading control (lower panel). (E) Effects of ectopic expression of WT-SphK2-V5 and SphK2<sup>G212E</sup>-V5 on caspase 3

activation were measured by immunofluorescence using anti-caspase 3 antibody that detects activated caspase 3 compared to empty vector-V5 in A549 cells. Images were quantified using ImageJ (right panel). Data are means  $\pm$  SD from three independent experiments, analysed by student's t-test ( $n=3$ ,  $*P=0.003$ ,  $**P=0.472$ ,  $***P=0.0002$ ). Scale bars represent 100  $\mu\text{m}$ . (F) Effects of exogenous S1P exposure (using BSA-conjugated S1P, 5 $\mu\text{M}$ ) on caspase 3 activation in the absence/presence of ABC294640 were measured in A549 cells compared to vehicle-treated controls. Data are means  $\pm$  SD from three independent experiments, analysed by student's t-test ( $n=3$ ,  $*P=0.008$ ,  $**P=0.006$ ).

**Fig. 3. Silencing SPHK2 or hTERT induces telomere damage in A549 cells.** (A) Effects of genetic loss of SphK2 in inducing telomere damage were measured using TIF assay in MEFs isolated from SphK2<sup>-/-</sup> compared to WT mice by immunofluorescence. Images were quantified using ImageJ (right panel). Data are means  $\pm$  SD from three independent experiments, analysed by student's t-test ( $n=3$ ,  $*P=0.001$ ). Scale bars represent 100  $\mu\text{m}$ . (B-C) Effects of shRNA-mediated knockdown of SPHK2 (B) or hTERT in A549 cells on telomere damage in the absence/presence of ABC294640 (C) were measured using TIF assay by immunofluorescence. Images were quantified using ImageJ (upper right panel). Data are means  $\pm$  SD from three independent experiments, analysed by student's t-test ( $n=3$ ,  $*P=0.03$ ). Sh-RNA-mediated knockdown of hTERT mRNA was confirmed using qPCR compared to Scr-shRNA-transfected controls (lower left panel), data are means  $\pm$  SD from three independent experiments, analysed by student's t-test ( $n=3$ ,  $*P=0.047$ ) and TIF colocalization was quantified. Data are means  $\pm$  SD from three independent experiments, analysed by student's t-test ( $n=3$ ,  $*P=0.030$ ,  $**P=0.003$ ,  $***P=0.108$ ). Scale bars represent 100  $\mu\text{m}$ . (D) Effects of ABC294640 or cisplatin on p53-dependent DNA damage was measured by immunofluorescence using anti- $\gamma\text{H2AX}$  and anti-p53 antibodies in A549 cells compared to vehicle (DMSO)-treated controls. Images were quantified using ImageJ (right panel). Data are means  $\pm$  SD from three independent experiments, analysed by

student's t-test ( $n=3$ ,  $*P=0.031$ ,  $**P=0.605$ ). Scale bars represent 100  $\mu\text{m}$ .

**Fig. 4. S1P-hTERT binding protects caspase 3 activation in response to ABC294640 by phospho-mimicking of hTERT by S1P at S921.** (A-B) Effects of ectopic expression of WT-hTERT, hTERT<sup>D684A</sup>, hTERT<sup>S921D</sup> and hTERT<sup>S921D-D684A</sup> on caspase 3 activation in the absence/presence of ABC294640 were measured in GM847 cells using immunofluorescence (A). Images were quantified by ImageJ (B). Data are means  $\pm$  SD from three independent experiments, analysed by student's t-test ( $n=3$ ,  $*P=0.052$ ,  $**P=0.010$ ). Scale bars represent 100  $\mu\text{m}$ . (C) Association of S1P with S921D-hTERT and S921D-D684A-hTERT compared to vector-transfected GM847 cells was measured by PLA using anti-S1P (Sphingomab) and anti-hTERT antibodies. Data are means  $\pm$  SD from three independent experiments, analysed by student's t-test ( $n=3$ ,  $*P=0.00064$ ,  $**P=0.0028$ ,  $***P=0.0028$ ). Scale bars represent 100  $\mu\text{m}$ . (D) Ectopic expression of WT-, D684A-, S921A, S921A/D684A-, S921D-, and S921D-D684A-hTERT proteins in the presence/absence of ABC294640 in GM847 cells were confirmed by Western blotting using anti-hTERT antibody. Vector-transfected cell extracts were used as negative controls (right panel). Actin was used as a loading control (lower panel). Images represent at least three independent studies.

**Fig. 5. ABC294640-mediated telomere damage is prevented by the S1P-hTERT complex due to phospho-mimicking function of S1P at S921 of hTERT.** (A-B) Effects of ectopic expression of WT-, D684A-, S921A, S921A-D684A-, S921D-, and S921D-D684A-hTERT proteins on telomere damage in the presence/absence of ABC294640 in GM847 cells were detected by immunofluorescence using TIF assay (A). Scale bars represent 100  $\mu\text{m}$ . Images were quantified by ImageJ (B). Data are means  $\pm$  SD from three independent experiments, analysed by student's t-test ( $n=3$ ,  $*P=0.046$ ,  $**P=0.037$ ,  $***P=0.033$ ). (C) Effects of ectopically expressed WT-, D684A-, S921A, S921A-D684A-, S921D-, and S921D-D684A-hTERT proteins on GM847 cell viability in the absence/presence of ABC294640 were measured by trypan blue exclusion assay. Data are

means  $\pm$  SD from three independent experiments, analysed by student's t-test (n=3, \* $P$ =0.046, \*\* $P$ =0.051, \*\*\* $P$ =0.044).

**Fig. 6. Effects of TCF21 silencing on ABC294640-mediated tumor suppression in mice.** (A-D) Effects of shRNA-dependent silencing of TCF21 on A459 xenograft-derived tumor growth in the presence/absence of ABC294640 (n=4 mice per group, each containing two tumors on both flanks) were measured in SCID mice for 21 days. Tumor growth was measured every alternative day for up to 21 days by calipers. After the growth study was completed, the tumors were removed and measured *ex vivo*. Two-way ANOVA with Tukey's posthoc test was performed. shScr Vs ShScr+ABC(\* $P$ <0.001,  $F$ =6.195,  $DF$ =30), shScr Vs shTCF21(\*\* $P$ =0.275), shTCF21 Vs shTCF21+ABC(\*\*\* $P$ =0.872) (A). Protein abundance of hTERT (n=3, \* $P$ =0.0478, \*\* $P$ =0.0346 by student's t-test) (B), activation of caspase 3 (C), and induction of apoptosis (D) in tumors were measured by Western blotting using anti-hTERT antibody, IHC using anti-active caspase 3 antibody, or TEM, respectively. (E) ShRNA-mediated knockdown of TCF21 using two distinct shRNAs (#1 or #2) in the absence/presence of ABC294640 was measured by qPCR in A549 cells. Data are means  $\pm$  SD from three independent experiments, analysed by student's t-test (n=3, \* $P$ =0.015, \*\* $P$ =0.422, \*\*\* $P$ =0.054). (F-G) Effects of TCF21 silencing using shRNA on telomere damage in the absence (F) or presence (G) of ABC294640 (ABC) were measured by TIF assay using anti-gamma-H2AX and TRF-2 antibodies by immunofluorescence. Data represent at least three independent experiments. Scr-shRNA and/or vehicle-treated cells were used as controls. Images were quantified using Image J. Scale bars represent 100  $\mu$ m.

**Fig. 7. Genetic loss of SphK2 results in accelerated senescence and aging in mice.** (A) Senescence was detected using SA-beta-gal staining in the paws of WT, SphK1<sup>-/-</sup> and SphK2<sup>-/-</sup> mice at generation 5. (B) Testes were isolated and weighed from WT, SphK1<sup>-/-</sup> and SphK2<sup>-/-</sup> mice at generations 4 and 5 (G4-G5). One-way ANOVA with Tukey's posthoc analysis test was performed (WT Vs SphK2<sup>-/-</sup> (\* $P$ <0.0001) and SphK1<sup>-/-</sup> Vs

SphK2<sup>-/-</sup> (\*\* $P$ <0.0001) with  $F$ =18.91 and  $DF$ =76. (C) Spleen, skin and testes tissues from WT and SphK2<sup>-/-</sup> mice at generation 5 were isolated and examined after H&E staining. (D) Apoptosis was detected by TUNEL staining in testes tissues isolated from WT and SphK2<sup>-/-</sup> mice at generation 4 (G4, upper panel). Protein abundance of mTERT and tcf21 were detected by IHC using anti-mTERT and anti-tcf21 antibodies in testes tissues isolated from WT, SphK1<sup>-/-</sup> and SphK2<sup>-/-</sup> mice at generation 4 (G4, lower panels). (E) Telomere damage in testes isolated from G4 of WT, SphK1<sup>-/-</sup> and SphK2<sup>-/-</sup> mice was measured using TIF assay. Scale bars represent 100  $\mu$ m. All mice were between 6-8 weeks old.

**Fig. 8. Genetic loss of SphK2 results in accelerated p16-dependent senescence but not apoptosis via increased telomere damage in non-cancerous fibroblasts.** (A) Senescence in testes tissues obtained from WT and SphK2<sup>-/-</sup> mice at generations 4, 5 and 6 was measured by SA-beta-gal staining. Scale bars represent 100  $\mu$ m. (B) Abundance of p16 mRNA was measured by qPCR in MEFs isolated from WT, SphK1<sup>-/-</sup> and SphK2<sup>-/-</sup> mice at generations 6 in the absence/presence of Scr- or p16-shRNAs. Data are means  $\pm$  SD from three independent experiments, analysed by student's t-test (n=3, \* $P$ =0.0402, \*\* $P$ =0.0019) (C-D) Effects of p16 knockdown on telomere damage (C), Data are means  $\pm$  SD from three independent experiments, analysed by student's t-test (n=3, \* $P$ =0.006, \*\* $P$ =0.013) or caspase 3 activation (D) were measured using immunofluorescence in MEFs obtained from WT, SphK1<sup>-/-</sup>, and SphK2<sup>-/-</sup> mice at generation 6. Scr-shRNA transfected SphK2<sup>-/-</sup> MEFs were used as controls. Images were quantified using ImageJ (right panels). Data are means  $\pm$  SD from three independent experiments, analysed by student's t-test (n=3, \* $P$ =0.001).

**Fig. 9. Reconstitution of p16 induces senescence and prevents apoptosis in cancer cells in response to ABC294640-mediated SPHK2 inhibition and telomere damage.** (A) Effects of stable expression of p16 on caspase 3 activation in A549 cells transfected with Scr- or SPHK2-shRNAs were measured by immunofluorescence. Images were quantified by ImageJ (lower panel). Data are means  $\pm$  SD from three independent

experiments, analysed by student's t-test (n=3, \* $P=0.001$ , \*\* $P=0.0005$ , \*\*\* $P=0.0004$ ). Expression levels of p16 protein in stable shSPHK2 Vs shScr A549 cells were confirmed by Western blotting using anti-p16 antibody (Upper right panel). Actin was used as a loading control (Lower right panel). **(B-C)** Effects of stable expression of p16 on senescence in response to shRNA-knockdown **(B)** or ABC294640-mediated inhibition **(C)** of SPHK2 were measured by SA-beta-gal staining in A549 cells compared to Scr-transfected and/or vehicle-treated controls. **(D-E)** Effects of stable expression of p16 on telomere damage **(D)**, Images were quantified by ImageJ, Data are means  $\pm$  SD from three independent experiments, analysed by student's t-test (n=3, \* $P=0.006$ , \*\* $P=0.002$ ) or caspase 3 activation **(E)** in A549 cells in the absence/presence of ABC294640 were measured using TIF assay or caspase 3 activation assay by immunofluorescence and confocal microscopy. Images were quantified by ImageJ (right panels). Data are means  $\pm$  SD from three independent experiments, analysed by student's t-test (n=3, \* $P=0.0006$ , \*\* $P=0.0005$ , \*\*\* $P=0.0004$ ). **(F)** ShRNA-mediated knockdown of p16 was confirmed using qPCR in H1341 cells compared to Scr-shRNA-transfected controls. Data are means  $\pm$  SD from three independent experiments, analysed by student's t-test (n=3, \* $P=0.00005$ ). **(G)** Caspase 3 activation was measured by immunofluorescence using anti-caspase 3 antibody that detects active-caspase 3 in H1341 with/without p16 knockdown compared to Scr-shRNA-transfected controls in the absence/presence of ABC294640 (right panel). Effects of ectopic expression of p16 on caspase 3 activation in the presence/absence of ABC294640 was measured in A549 cells compared to vector-transfected controls (left panel). **(H)** Expression levels of p16 protein in different lung cancer cell lines were confirmed by Western Blotting using anti-p16 antibody (upper panel). Actin was used as a loading control (lower panel).

**Fig. 10. Interaction between p16 and caspase 3 prevents apoptosis and induces senescence in response to telomere damage.** **(A)** Association between endogenous p16 and caspase 3 was measured using PLA in H1341 cells in the absence/presence of Scr- or p16-shRNAs. Quantification of PLA images were performed

using the PLA software as described by the manufacturer. Data are means  $\pm$  SD from three independent experiments, analysed by student's t-test (n=3, \* $P=0.0349$ ). Successful knockdown of p16 using shRNA was confirmed by Q-PCR in H1341 cells compared to Scr-shRNA-transfected cells (right panel). Data are means  $\pm$  SD from three independent experiments, analysed by student's t-test (n=3, \* $P=0.004$ ). **(B-C)** Interaction and co-localization of p16 and caspase 3 in response to SPHK2 inhibitor ABC294640 (ABC) in the absence/presence of ectopic expression of WT-p16 (p16) and/or shRNA-dependent knockdown of SPHK2 (shSPHK2) were measured using PLA. Data are means  $\pm$  SD from three independent experiments, analysed by student's t-test (n=3, \* $P=0.045$ , \*\* $P=0.094$ , \*\*\* $P=0.005$ ) **(B)** or confocal microscopy and immunofluorescence **(C)** in A549 cells. Data are means  $\pm$  SD from three independent experiments, analysed by student's t-test (n=3, \* $P=0.484$ , \*\* $P=0.001$ , \*\*\* $P=0.0009$ , \*\*\*\* $P=0.001$ ). Vehicle-treated, vector-only or Scr-shRNA-transfected cells were used as controls. Data represent at least three independent studies. Quantification of PLA images were performed using the PLA software as described by the manufacturer. Quantification of co-localization was performed using Image J. ShRNA-mediated knockdown of SPHK2, and ectopic expression of WT-p16 were confirmed using Q-PCR(upper panels) and Western blotting respectively (lower panels). Data are means  $\pm$  SD from three independent experiments, analysed by student's t-test (n=3, \* $P=0.049$ ). **(D)** Molecular modeling for the predicted interaction between p16 and caspase 3 was generated using already existing NMR structure of p16 and crystal structure caspase 3 as described in Materials and Methods. Ser<sup>152</sup> of p16 (turquoise) and Gly<sup>251</sup> of caspase 3 (grey) were among key residues for the interaction between these two proteins. **(E)** Association between p16 and caspase 3 was measured by PLA in A549 cells expressing WT-p16 or p16<sup>S152A</sup> in the absence/presence of ABC294640. Vector-only-transfected and vehicle-treated cells were used as controls. Data are means  $\pm$  SD from three independent experiments, analysed by student's t-test (n=3, \* $P=0.010$ , \*\* $P=0.009$ , \*\*\* $P=0.009$ ). Quantification of PLA images were performed using the PLA software as described by the manufacturer. **(F-G)** Effects of ABC294640

exposure on caspase 3 activation were measured by confocal microscopy and immunofluorescence using anti-caspase 3 antibody that detects activated caspase 3 in A549 cells expressing WT-p16 or p16<sup>S152A</sup> (F). Data are means ± SD from three independent experiments, analysed by student's t-test (n=3, \*P=0.0001, \*\*P=0.643, \*\*\*P=0.0006). Vector-only-transfected and vehicle-treated cells were used as controls. Quantification of co-localization was performed using Image J. Expression of WT-p16 and p16<sup>S152A</sup> was confirmed by Western blotting (G). Vector-transfected cell extracts were used as controls. (H) Association between p16 and caspase 3 was measured by PLA in testes tissues obtained from WT (SphK1<sup>+/+</sup>/SphK2<sup>+/+</sup>), SphK1-deficient (SphK1<sup>-/-</sup>) or SphK2-deficient (SphK2<sup>-/-</sup>) mice at generation 6. Data are means ± SD from three independent experiments, analysed by student's t-test (n=3, \*P=0.002, \*\*P=0.001). Quantification of PLA images were performed using the PLA software as described by the manufacturer. Scale bars represent 100 µm.

**Fig. 11. Graphical summary.** Our data suggest that SPHK2-generated S1P binds and stabilizes TERT involving its D684 residue via mimicking TERT phosphorylation at S921, which protects telomere damage, and results in delayed senescence and protection from apoptosis. Our data also suggest that targeting/inhibition of the SPHK2/S1P/telomerase axis results in telomere damage, which signals TCF21-dependent caspase 3 activation in cancer cells or immortalized MEFs, or p16-dependent senescence and accelerated aging phenotype in non-cancerous primary lung fibroblasts, primary MEFs, or non-cancerous tissues, such as testes, of subsequent generations of SphK2<sup>-/-</sup> mice. Thus, these data reveal that p16 abundance induces senescence and prevents caspase-3-dependent apoptosis in response to telomere damage via p16-caspase 3 interaction in response to targeting the SPHK2/S1P/telomerase axis.

## SUPPLEMENTAL FIGURE LEGENDS

**Supplemental Figure 1. Targeting SPHK2 using ABC294640 inhibits orthotopic A549 xenograft-derived lung tumors and hTERT abundance.**

(A) Chemical structure of ABC294640. (B-C) Effects of inhibition of SPHK2 using ABC294640 on A549-luciferase xenograft-derived lung tumors (100 mg/kg for 14 days) established orthotopically in lungs of SCID mice (n=7 mice per group) after tail vein injections (1 X10<sup>6</sup> cells). Images were obtained and quantified (B-C) using Xenogen IVIS 200 Bioluminescence and Fluorescence Imaging System. \*P=0.05 by student t-test. (D) Effects of ABC294640 on cell proliferation and hTERT abundance in lung tumor tissues (shown in B-C) were detected by IHC using anti-Ki-67 and anti-hTERT antibodies. Scale bars represent 100 µm.

**Supplemental Figure 2. Increased SPHK2 and hTERT protein abundance is detected in lung tumor tissues obtained from patients.** (A) Expression of SPHK2 in lung tumor tissues obtained from patients (n=5) compared to their matched non-cancerous adjacent lung tissues (n=5) were detected by IHC using anti-SPHK2 antibody. Scale bars represent 100 µm. (B) Expression of SPHK2 (left panel) and hTERT (right panel) in NSCLC tissues (n=48) in TMAs containing lung tumors (T), adjacent non-cancerous lung tissues (AN, n=48), and normal lung tissues (n=4) was detected by IHC using anti-SPHK2 and anti-hTERT antibodies. Scale bars represent 100 µm. Statistical analyses of the data were performed using paired t-test (P<0.0001). (C) Co-expression of SPHK2 and hTERT in NSCLC tumors (n=96) in TMAs (shown in B) was analyzed using paired t-test. (D) Expression of SPHK2 (left panel) and hTERT (right panel) in SCLC tissues (n=40) in TMAs containing lung tumors (T), and normal lung tissues (N, n=10) was detected by IHC using anti-SPHK2 and anti-hTERT antibodies. Statistical analyses of the data (shown in D) were performed using the Wilcoxon ran sum test, \*P=0.0012, \*\*P=0.031 (right panels).

**Supplemental Figure 3. Inhibition or shRNA-mediated knockdown of SPHK2 induces telomere damage and caspase 3 activation in growth arrested A549 cells.** (A-B) Effects of ABC294640 (ABC) (A) or shRNA-mediated knockdown of SPHK2 (B) on telomere damage (upper panels) using TIF assay, and caspase 3 activation using anti-caspase 3 antibody that

detects activated caspase 3 (lower panels) in growth arrested A549 cells in response to serum starvation were measured by immunofluorescence. Data represent at least three independent experiments. (C-E) Cell cycle profiles of A549 cells in response to serum starvation (C-D) compared to controls, cells grown in complete media with serum (E), with/without ABC294640, ABC (C) or shRNA-SPHK2, SK2 (D) were measured using flow cytometry. Data represent three independent experiments, and error bars represent standard deviation.

**Supplemental Figure 4. Effects of SPHK2 knockdown on ceramide, dihydro-ceramide and S1P were measured by lipidomics.** (A-B) Effects of shRNA-mediated knockdown of SPHK2, SK2 mRNA, measured by qPCR (A) on sphingolipids (n=4, \*P=0.02), such as ceramide, dihydro-C16-ceramide, sphingosine, dihydro-sphingosine, dihydro-S1P, or S1P were measured using mass spectrometry-based lipidomics (B) in serum starved and G0/G1 arrested A549 cells (n=6). Data are means ± SD (std dev) analyzed by student's t-test.

**Supplemental Figure 5. ABC294640 induces telomere damage but not caspase 3 activation in primary non-cancerous human lung fibroblasts.** Effects of ABC294640 on telomere damage (upper panel) and caspase 3 activation (lower panel) in human non-cancerous lung epithelial cells were measured using TIF assay and anti-caspase 3 antibody that recognizes activated caspase 3, respectively, were measured by immunofluorescence. Data represent at least three independent experiments.

**Supplemental Figure 6. Targeting SPHK2 induces TCF21-mediated apoptosis and lung tumor suppression.** (A) Effects of ABC294640-mediated SPHK2 inhibition in the abundance of genes involved in lung tumor growth or suppression in tissues obtained from SCID mice treated with ABC294640 compared to vehicle were measured by qPCR using Superarray. (B-C) Increase in TCF21 mRNA in response to SPHK2 (B) (n=3, \*P=0.016) or hTERT (n=3, \*P=0.024) (C) knockdown using shRNAs in A549 cells was measured by qPCR. ShRNA-mediated knockdown of SPHK2 or hTERT (lower panels in B and C,

respectively) were confirmed by qPCR in A549 cells compared to Scr-shRNA-transfected controls. Data are means ± SD from three independent experiments, analyzed by student's t-test (n=3, \*P=0.038). (D) Effects of ectopic expression of WT-hTERT or hTERT<sup>D684A</sup> on TCF21 mRNA in response to shRNA-mediated knockdown of SPHK2 compared to vector-and/or Scr-shRNA-transfected control A549 cells were measured by qPCR. Data are means ± SD from three independent experiments, analyzed by student's t-test. (n=3, \*P=0.0481, \*\*P=0.0174, \*\*\*P=0.0267) (E) Knockdown of TCF21 using shRNA was confirmed in A549 cells in the presence of ABC294640 compared to Scr-transfected controls by qPCR. Data are means ± SD from three independent experiments, analyzed by student's t-test (n=3, \*P=0.029, \*\*P=0.035). (F) Effects of shRNA-mediated knockdown of TCF21 on caspase 3 activation in the absence/presence of ABC294640 were measured by immunofluorescence using anti-caspase 3 antibody that detects activated caspase 3 in A549 cells. Images were quantified using ImageJ (bottom panel). Data are means ± SD from three independent experiments, analyzed by student's t-test (n=3, \*P=0.022, \*\*P=0.036, \*\*\*P=0.019). Scale bars represent 100 μm.

**Supplemental Figure 7. Recombinant purified p16 and caspase 3 proteins interact with each other *in vitro*.** (A) Association between recombinant purified p16 with caspase 3 (A) or mutant (pro) caspase 3 (B) was measured using SPR. (B) Purified caspase 3 protein is visualized by SDS-PAGE and Coomassie blue staining.

**Figure 1**

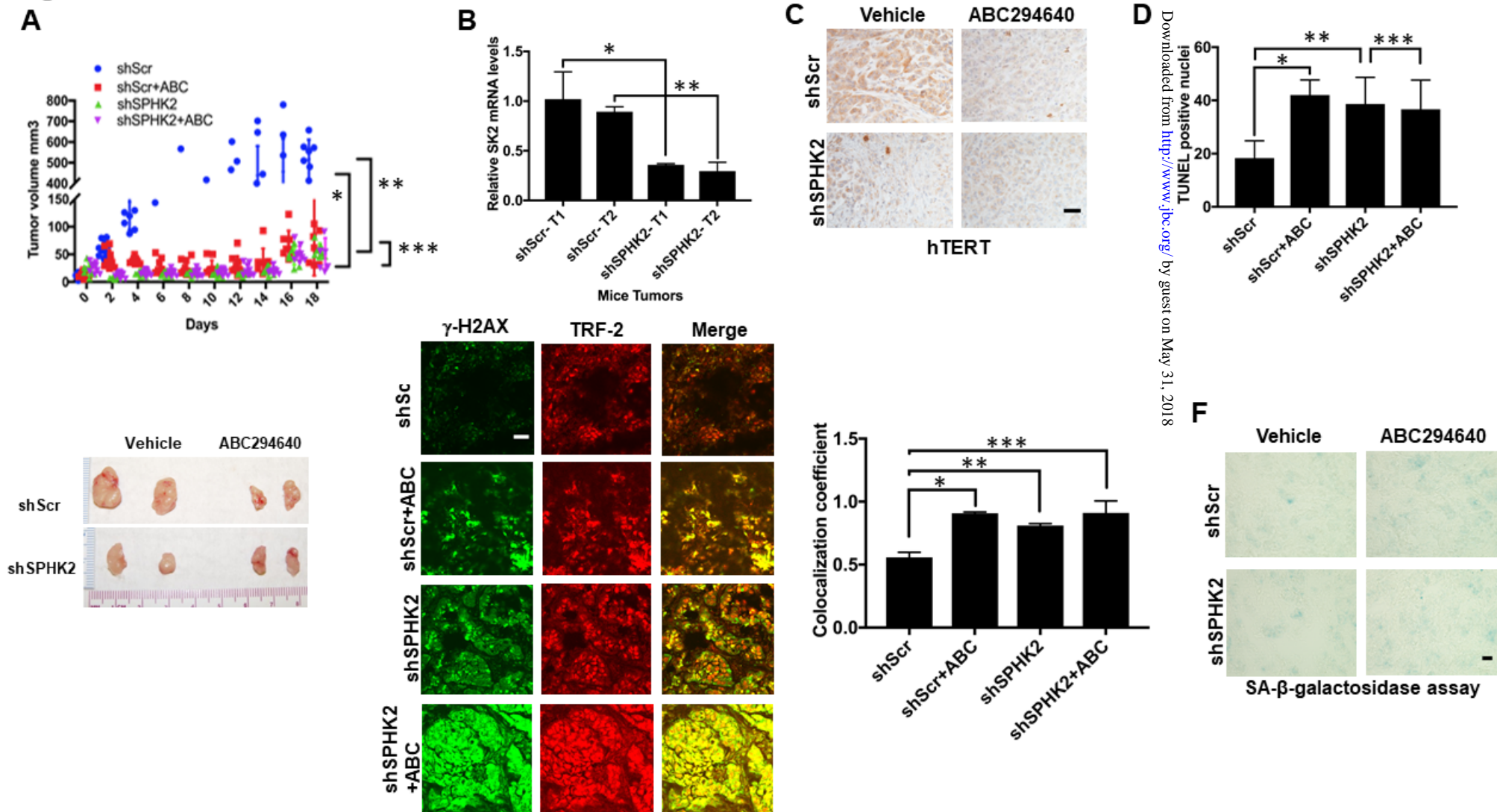


**Figure 2**

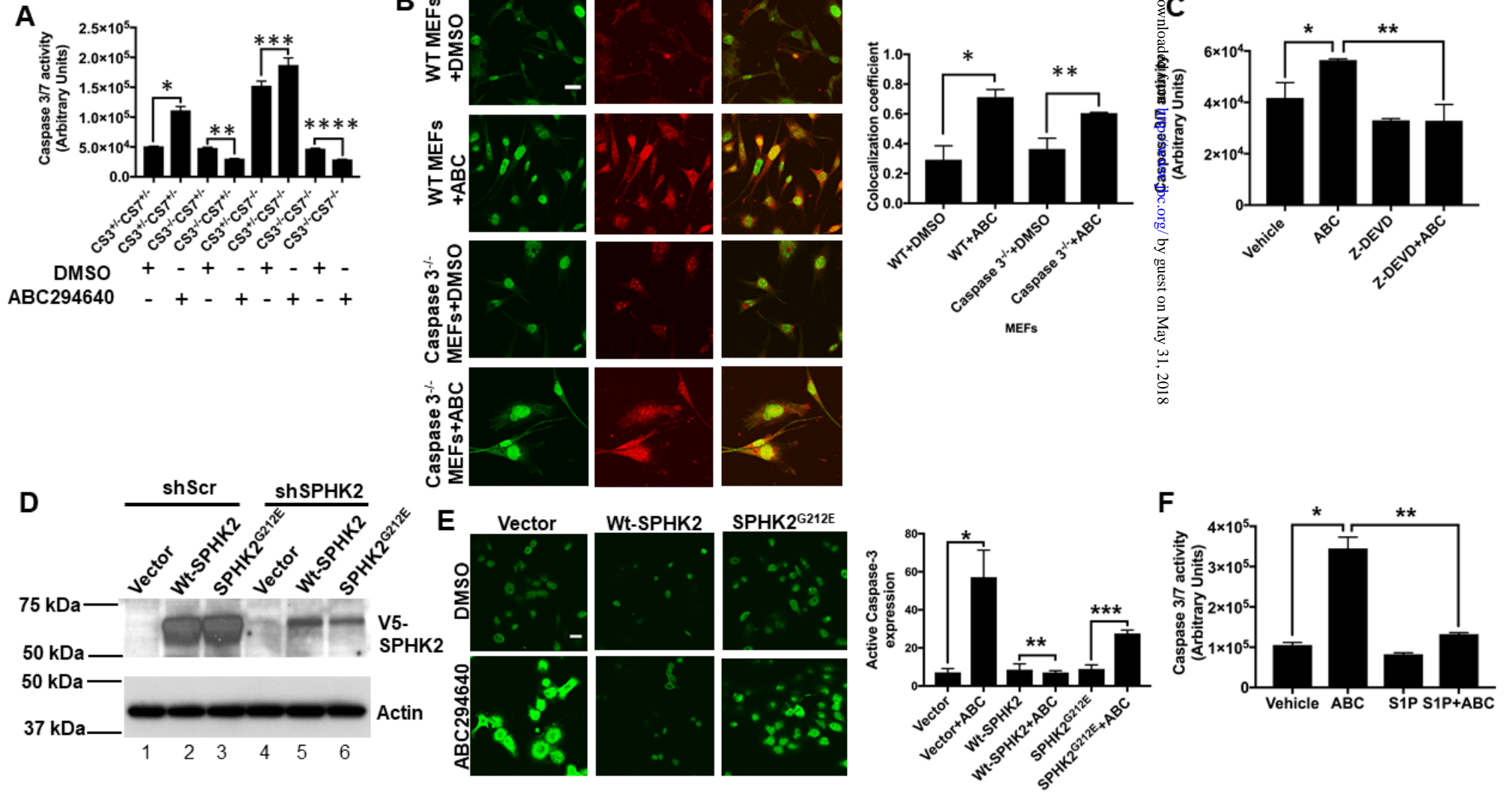


**Figure 3**

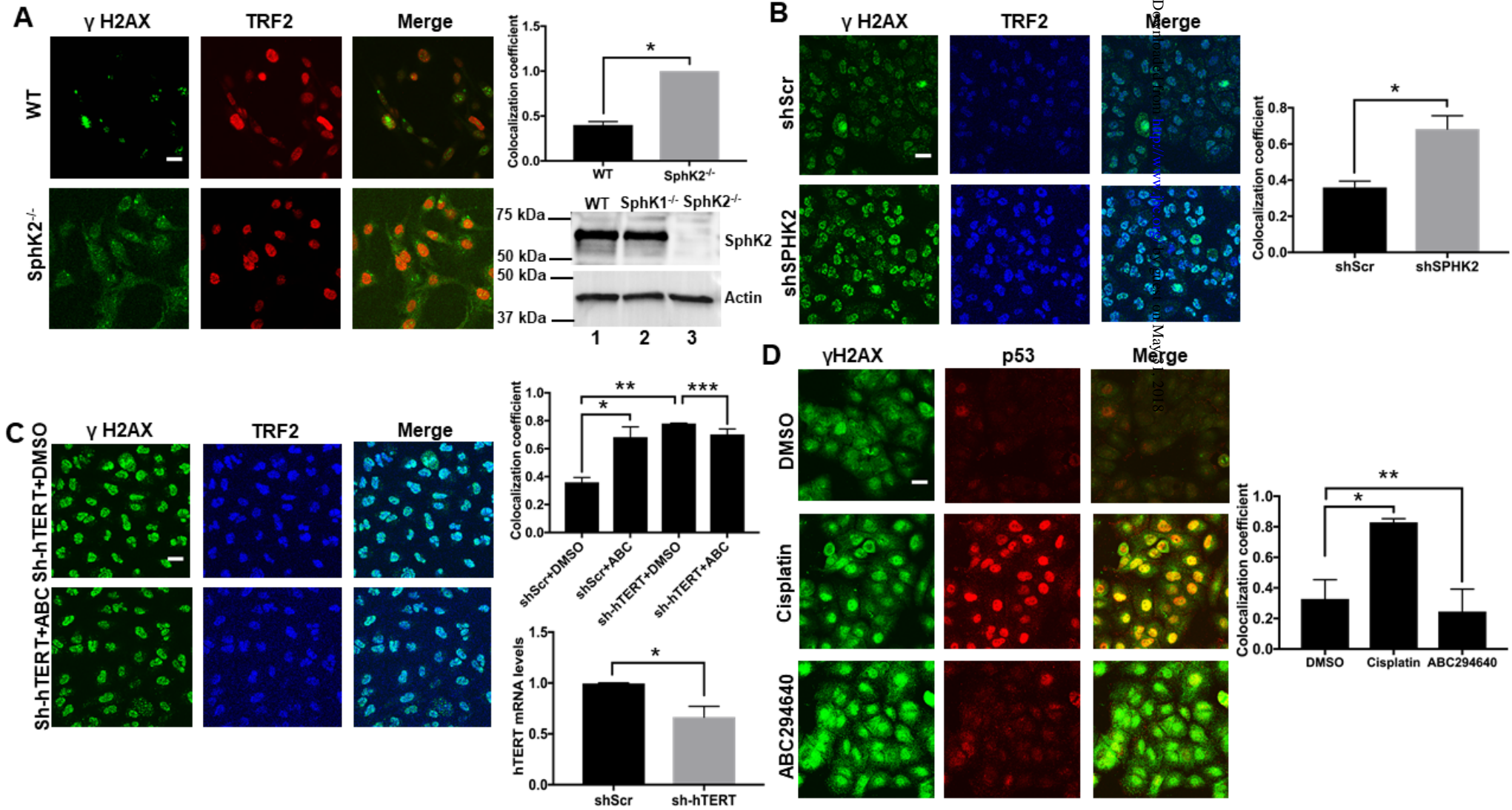


**Figure 4**

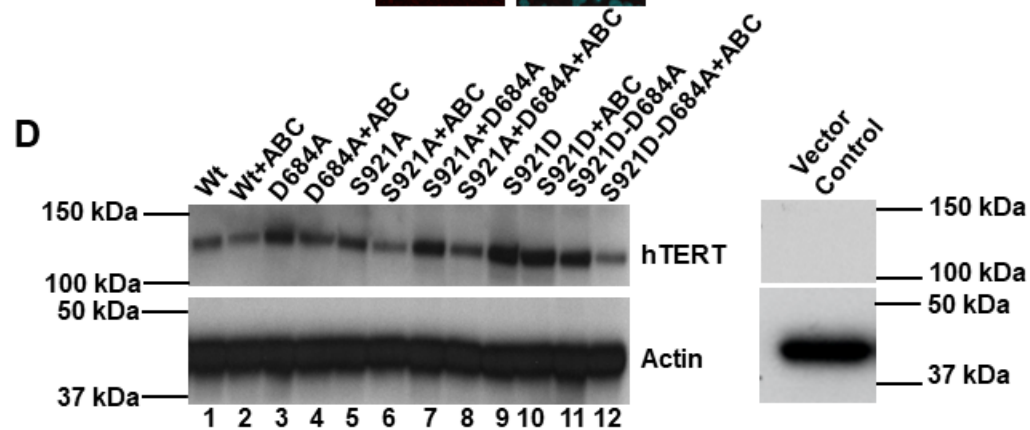
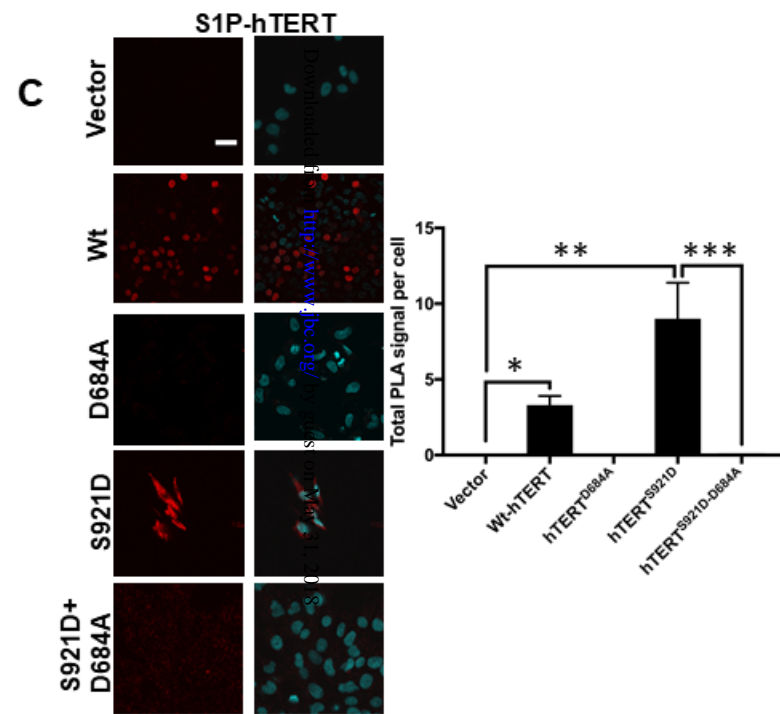
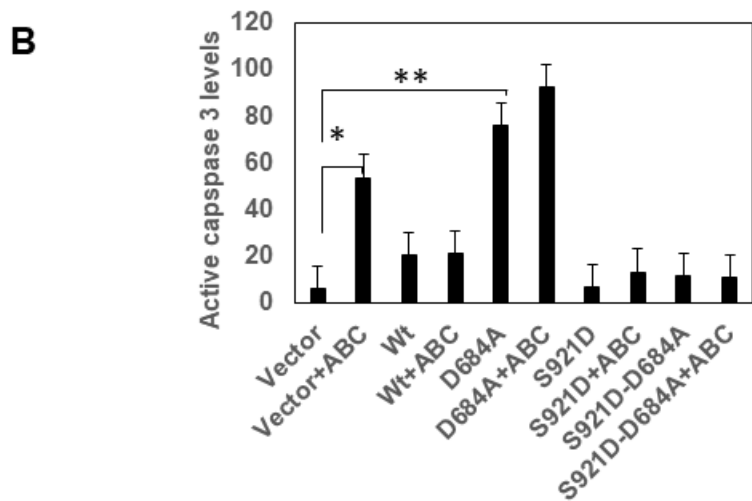
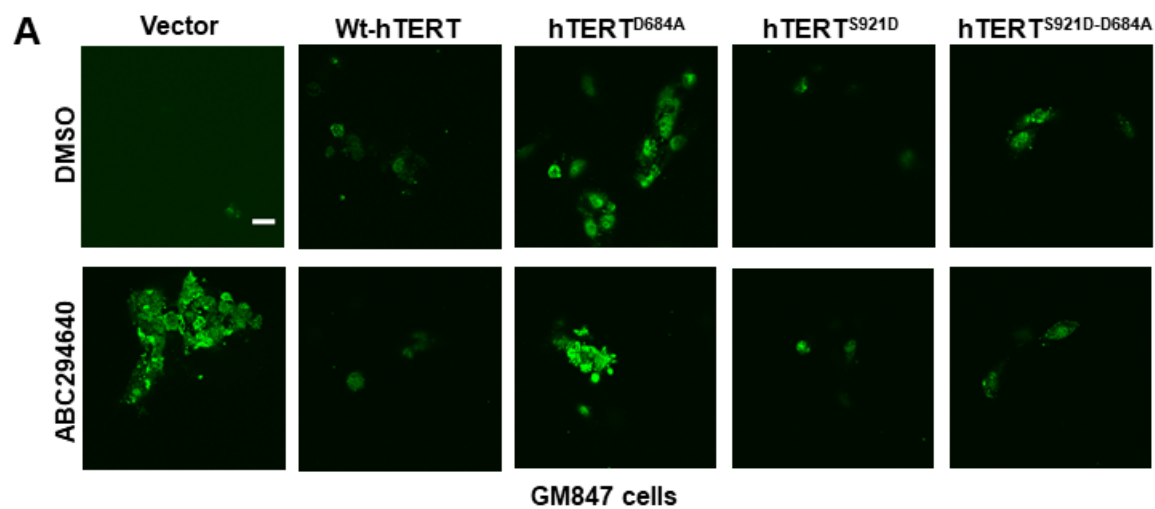


**Figure 5**

GM847 cells

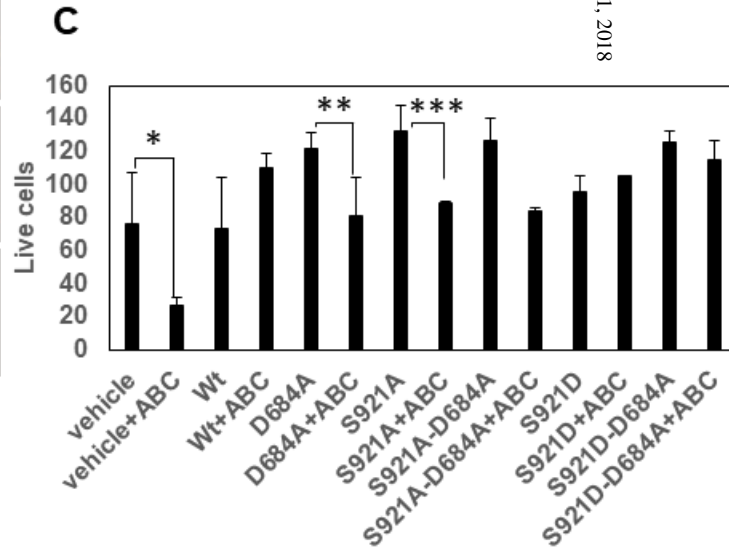
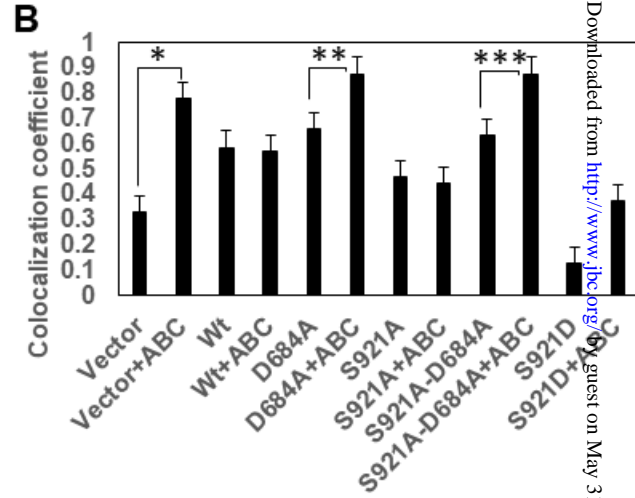
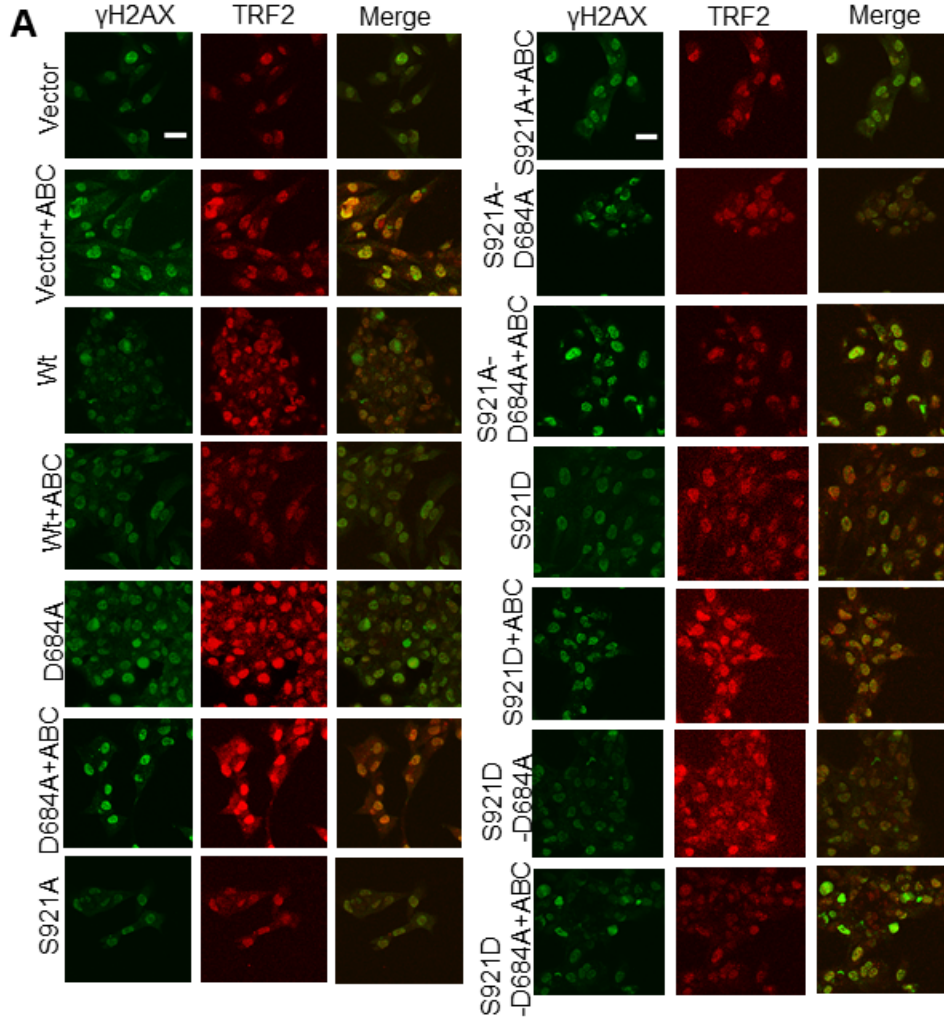


**Figure 6**

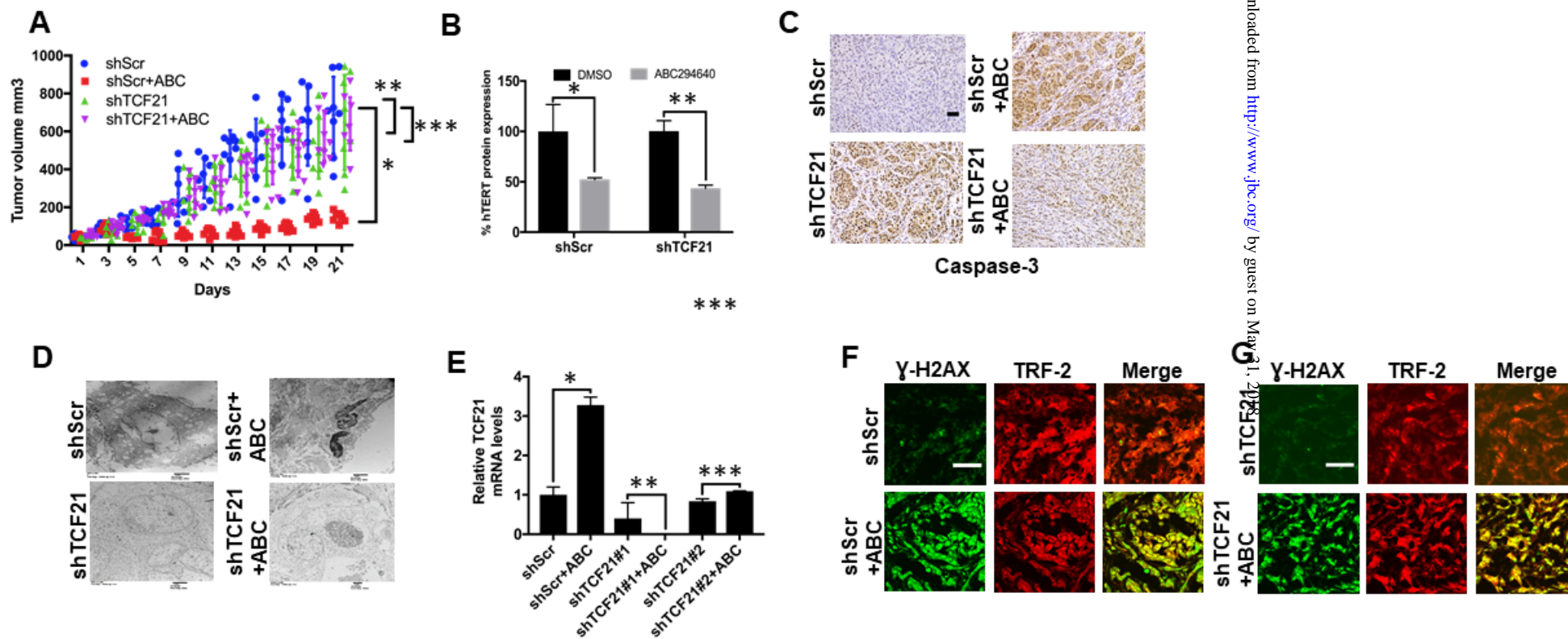
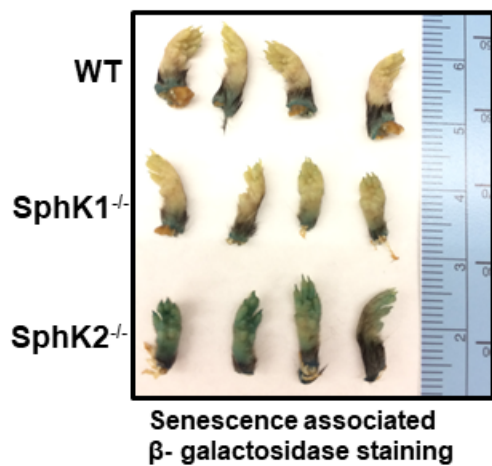
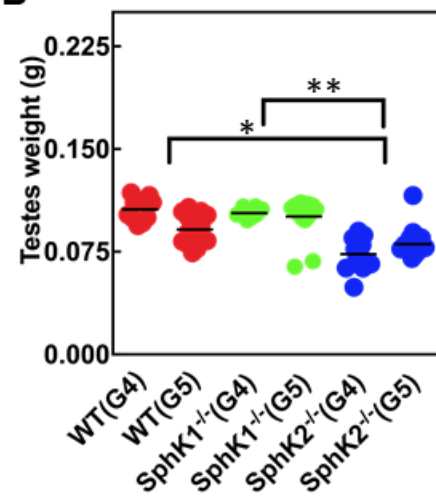


**Figure 7**

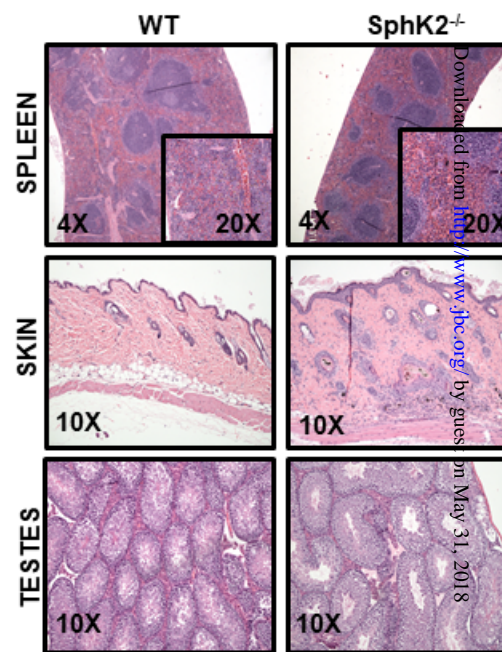
**A**



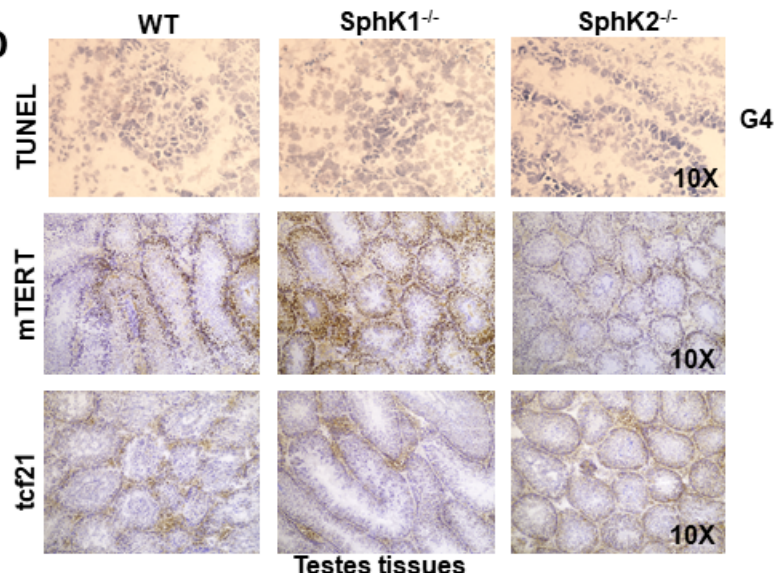
**B**



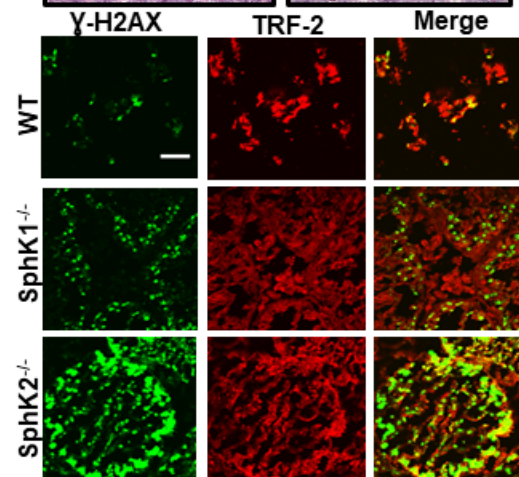
**C**



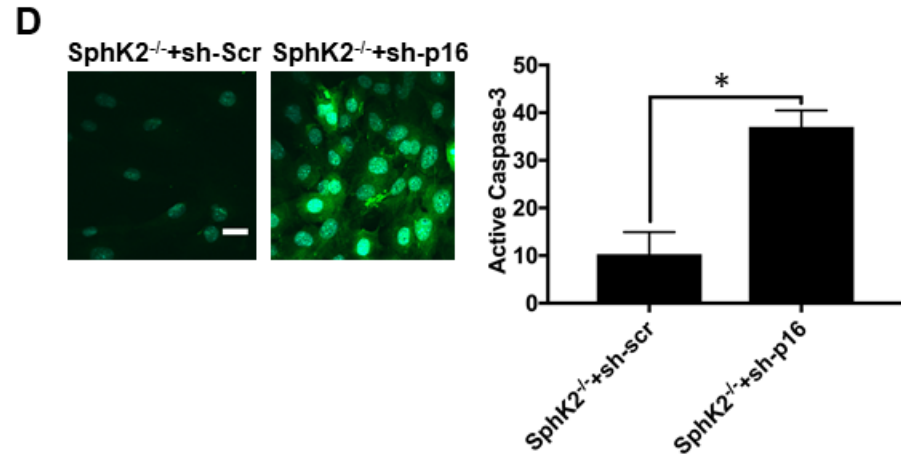
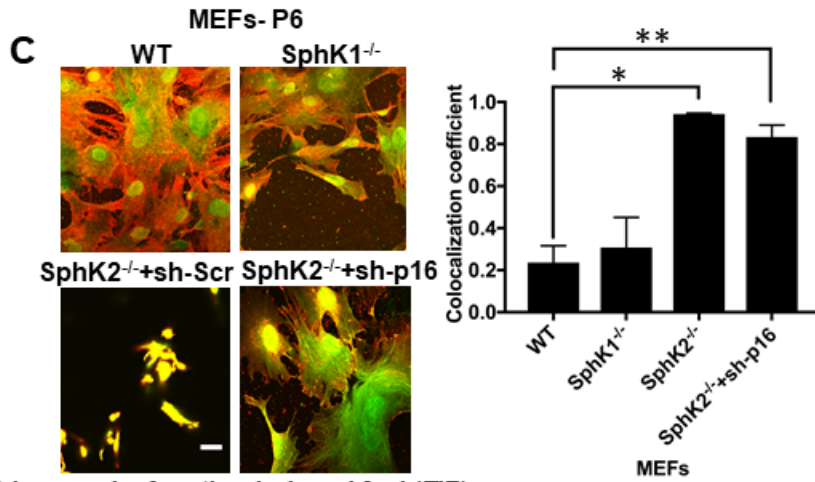
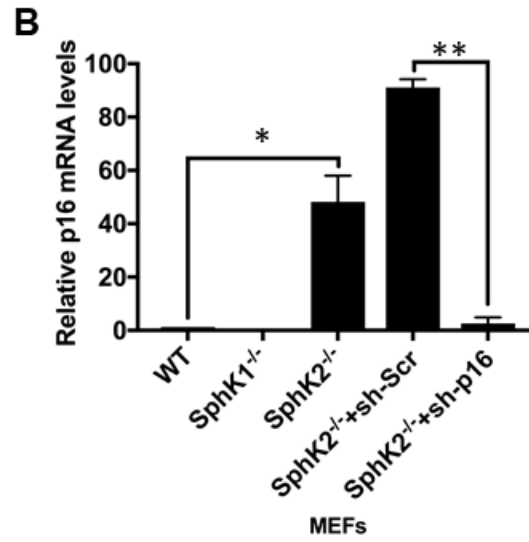
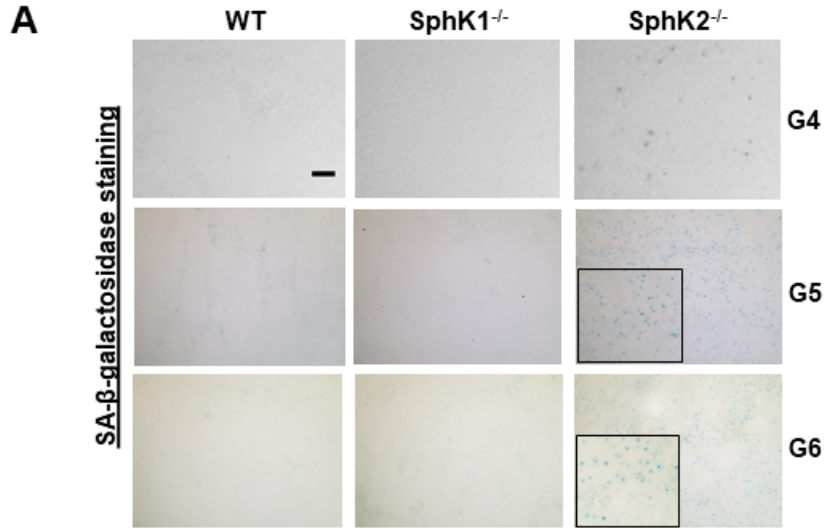
**D**



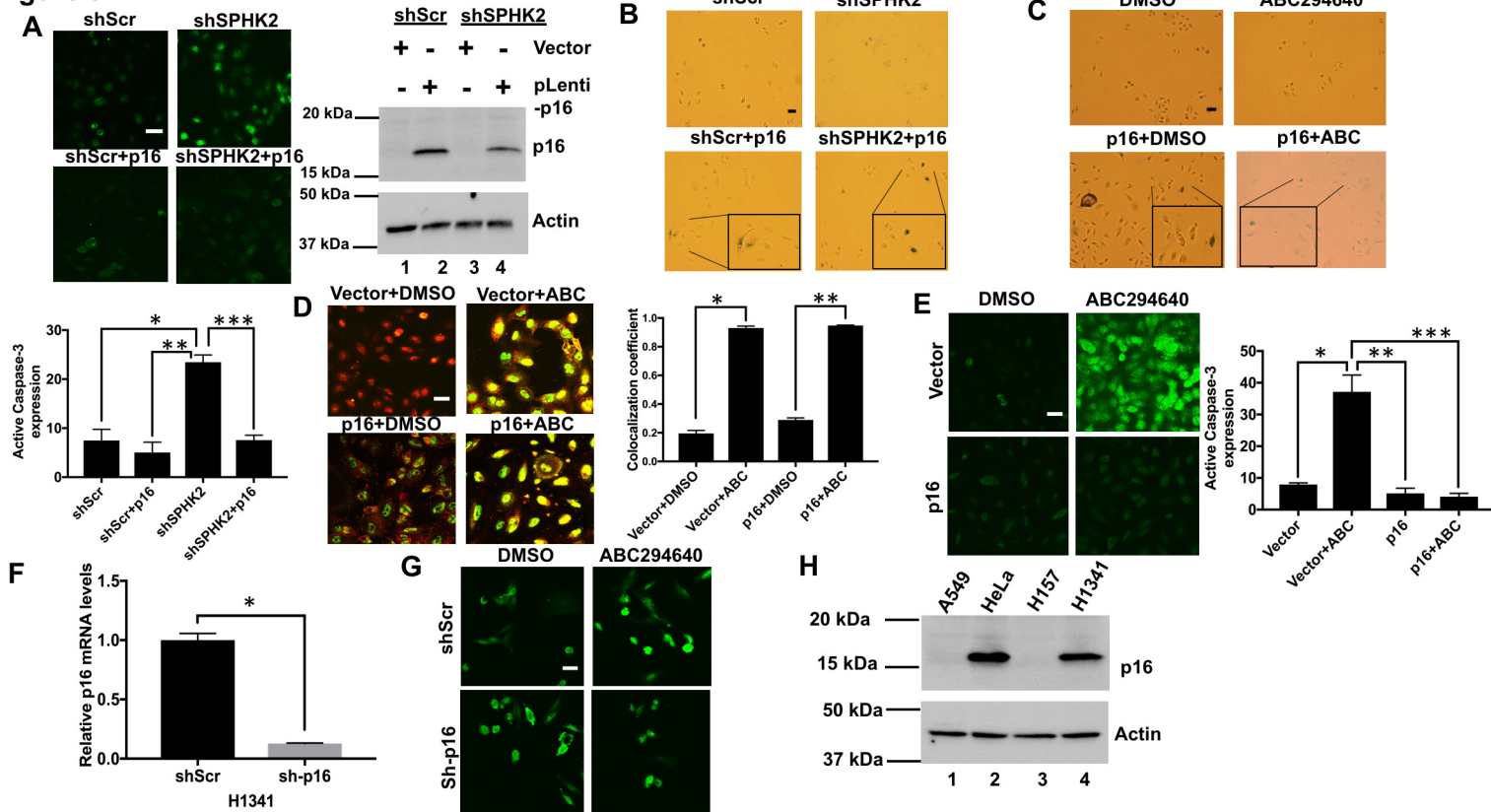
**E**



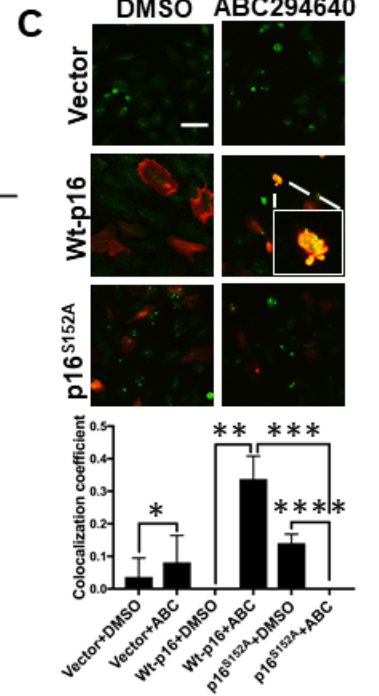
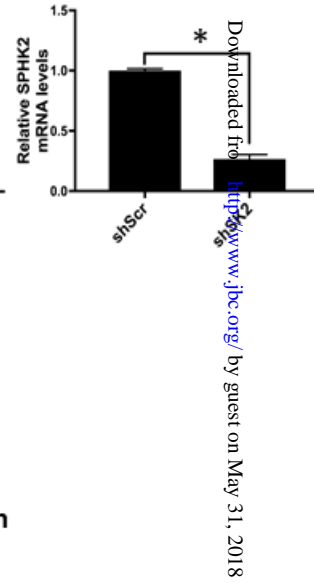
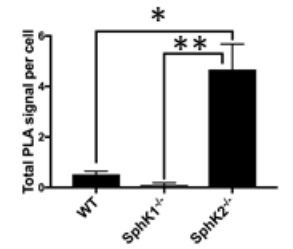
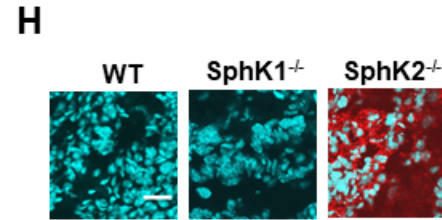
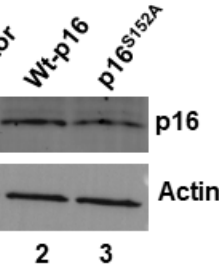
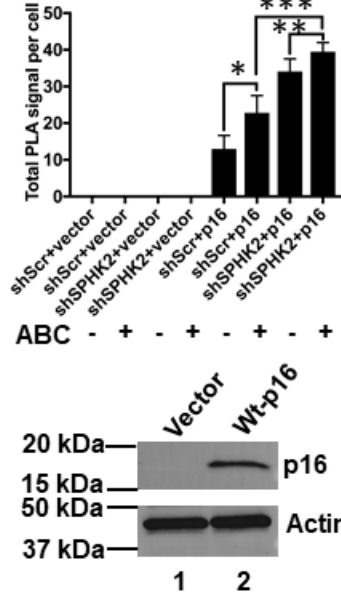
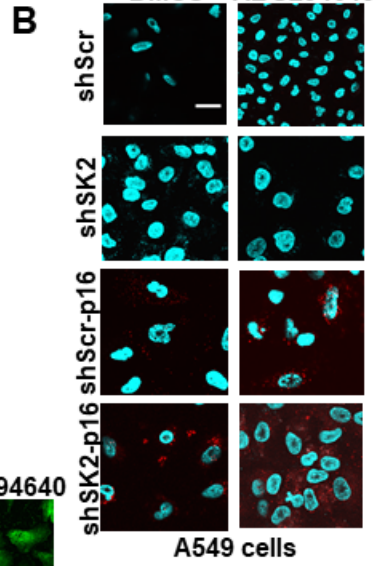
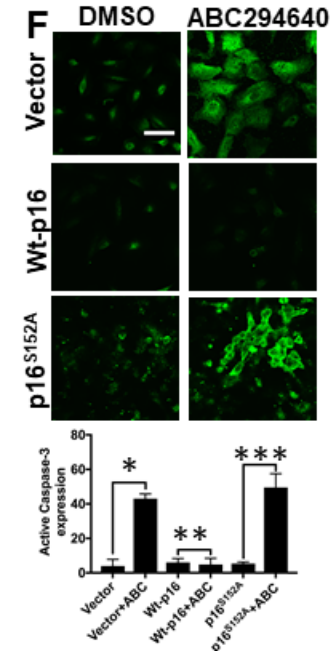
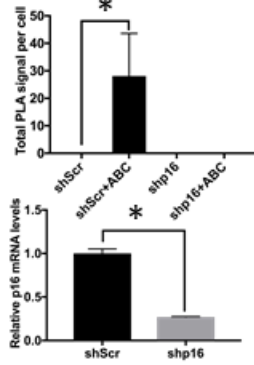
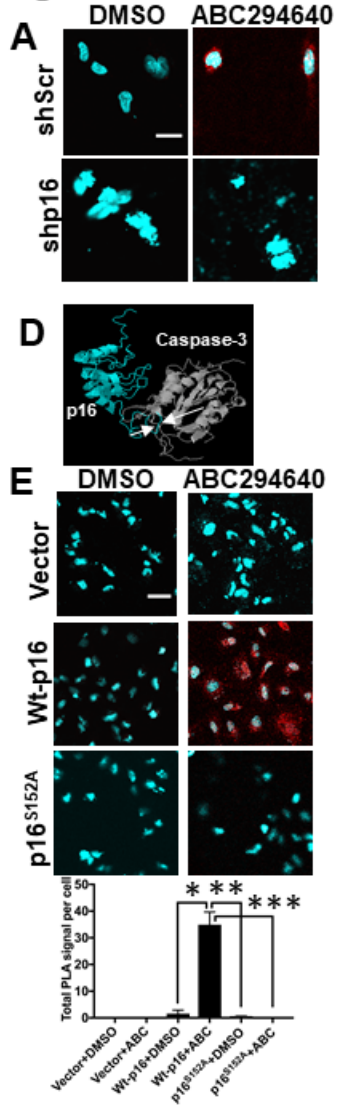
**Figure 8**



Telomere dysfunction induced foci (TIF) assay

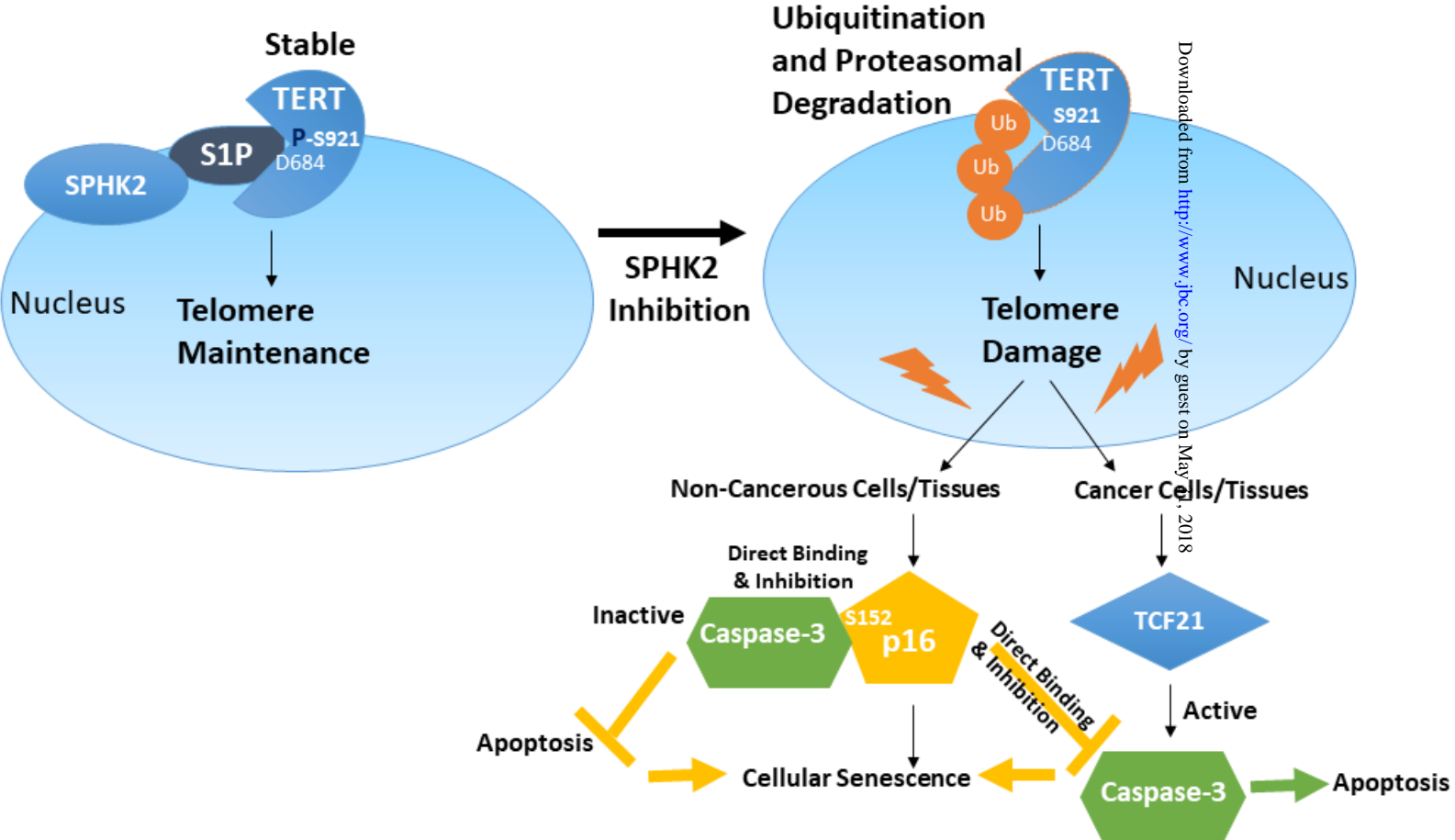
**Figure 9**

**Figure 10**



Downloaded from <http://www.jbc.org/> by guest on May 31, 2018

Figure 11



**Balance between senescence and apoptosis is regulated by telomere damage–induced association between p16 and caspase-3**

Shanmugam Panneer Selvam, Braden M Roth, Rose Nganga, Jisun Kim, Marion A Cooley, Kristi L. Helke, Charles D. Smith and Besim Ogretmen

*J. Biol. Chem.* published online May 10, 2018

---

Access the most updated version of this article at doi: [10.1074/jbc.RA118.003506](https://doi.org/10.1074/jbc.RA118.003506)

Alerts:

- [When this article is cited](#)
- [When a correction for this article is posted](#)

[Click here](#) to choose from all of JBC's e-mail alerts

## Supplemental Figures

Balance between senescence and apoptosis is regulated by telomere damage–induced association between p16 and caspase-3

Shanmugam Panneer Selvam<sup>1,2</sup>, Braden M. Roth<sup>1,2</sup>, Rose Nganga<sup>1,2</sup>, Jisun Kim<sup>1,2</sup>, Marion A. Cooley<sup>3,#</sup>, Kristi Helke<sup>4</sup>, Charles D. Smith<sup>5</sup>, and Besim Ogretmen<sup>1,2\*</sup>

<sup>1</sup>Department of Biochemistry and Molecular Biology, <sup>2</sup>Hollings Cancer Center, <sup>3</sup>Department of Regenerative Medicine, <sup>4</sup>Department of Comparative Medicine, Medical University of South Carolina, 86 Jonathan Lucas Street, Charleston, SC 29425; <sup>5</sup>Department of Pharmacology, Pennsylvania State University, 500 University Drive, Hershey, PA 17033.

#Current Address: Department of Oral Biology, Augusta University, Augusta, GA 30912.

\*Address correspondence to: [ogretmen@musc.edu](mailto:ogretmen@musc.edu)

### List of Supplemental Figures

Supplemental Figure 1. Targeting SPHK2 using ABC294640 inhibits orthotopic A549 xenograft-derived lung tumors and hTERT abundance.

Supplemental Figure 2. Increased SPHK2 and hTERT protein abundance is detected in lung tumor tissues obtained from patients.

Supplemental Figure S3. Inhibition or shRNA-mediated knockdown of SPHK2 induces telomere damage and caspase 3 activation in growth arrested A549 cells.

Supplemental Figure S4. Effects of SPHK2 knockdown on ceramide, dihydro-ceramide and S1P were measured by lipidomics.

Supplemental Figure S5. ABC294640 induces telomere damage but not caspase 3 activation in primary non-cancerous human lung fibroblasts.

Supplemental Figure 6. Targeting SPHK2 induces TCF21-mediated apoptosis and lung tumor suppression.

Supplemental Figure S7. Recombinant purified p16 and caspase 3 proteins interact with each other *in vitro*.

### SUPPLEMENTAL FIGURE LEGENDS

**Supplemental Figure 1. Targeting SPHK2 using ABC294640 inhibits orthotopic A549 xenograft-derived lung tumors and hTERT abundance.** (A) Chemical structure of ABC294640. (B-C) Effects of inhibition of SPHK2 using ABC294640 on A549-luciferase xenograft-derived lung tumors (100 mg/kg for 14 days) established orthotopically in lungs of SCID mice (n=7 mice per group) after tail vein injections (1 X10<sup>6</sup> cells). Images were obtained and quantified (B-C) using Xenogen IVIS 200 Bioluminescence and Fluorescence Imaging System. \*P=0.05 by student t-test. (D) Effects of ABC294640 on cell proliferation and hTERT abundance in lung tumor tissues (shown in B-C) were detected by IHC using anti-Ki-67 and anti-hTERT antibodies. Scale bars represent 100 μm.

**Supplemental Figure 2. Increased SPHK2 and hTERT protein abundance is detected in lung tumor tissues obtained from patients.** (A) Expression of SPHK2 in lung tumor tissues obtained from patients (n=5) compared to their matched non-cancerous adjacent lung tissues (n=5) were detected by IHC using

anti-SPHK2 antibody. Scale bars represent 100  $\mu\text{m}$ . **(B)** Expression of SPHK2 (left panel) and hTERT (right panel) in NSCLC tissues (n=48) in TMAs containing lung tumors (T), adjacent non-cancerous lung tissues (AN, n=48), and normal lung tissues (n=4) was detected by IHC using anti-SPHK2 and anti-hTERT antibodies. Scale bars represent 100  $\mu\text{m}$ . Statistical analyses of the data were performed using paired t-test ( $P<0.0001$ ). **(C)** Co-expression of SPHK2 and hTERT in NSCLC tumors (n=96) in TMAs (shown in B) was analyzed using paired t-test. **(D)** Expression of SPHK2 (left panel) and hTERT (right panel) in SCLC tissues (n=40) in TMAs containing lung tumors (T), and normal lung tissues (N, n=10) was detected by IHC using anti-SPHK2 and anti-hTERT antibodies. Statistical analyses of the data (shown in **D**) were performed using the Wilcoxon ran sum test,  $*P=0.0012$ ,  $**P=0.031$  (right panels).

**Supplemental Figure 3. Inhibition or shRNA-mediated knockdown of SPHK2 induces telomere damage and caspase 3 activation in growth arrested A549 cells.** **(A-B)** Effects of ABC294640 (ABC) (A) or shRNA-mediated knockdown of SPHK2 (B) on telomere damage (upper panels) using TIF assay, and caspase 3 activation using anti-caspase 3 antibody that detects activated caspase 3 (lower panels) in growth arrested A549 cells in response to serum starvation were measured by immunofluorescence. Data represent at least three independent experiments. **(C-E)** Cell cycle profiles of A549 cells in response to serum starvation (C-D) compared to controls, cells grown in complete media with serum (E), with/without ABC294640, ABC (C) or shRNA-SPHK2, SK2 (D) were measured using flow cytometry. Data represent three independent experiments, and error bars represent standard deviation.

**Supplemental Figure 4. Effects of SPHK2 knockdown on ceramide, dihydro-ceramide and S1P were measured by lipidomics.** **(A-B)** Effects of shRNA-mediated knockdown of SPHK2, SK2 mRNA, measured by qPCR (A) on sphingolipids (n=4,  $*P=0.02$ ), such as ceramide, dihydro-C16-ceramide, sphingosine, dihydro-sphingosine, dihydro-S1P, or S1P were measured using mass spectrometry-based lipidomics (B) in serum starved and G0/G1 arrested A549 cells (n=6). Data are means  $\pm$  SD (std dev) analyzed by student's t-test.

**Supplemental Figure 5. ABC294640 induces telomere damage but not caspase 3 activation in primary non-cancerous human lung fibroblasts.** Effects of ABC294640 on telomere damage (upper panel) and caspase 3 activation (lower panel) in human non-cancerous lung epithelial cells were measured using TIF assay and anti-caspase 3 antibody that recognizes activated caspase 3, respectively, were measured by immunofluorescence. Data represent at least three independent experiments.

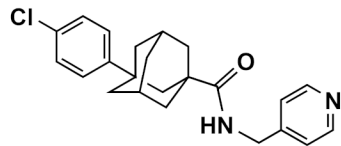
**Supplemental Figure 6. Targeting SPHK2 induces TCF21-mediated apoptosis and lung tumor suppression.** **(A)** Effects of ABC294640-mediated SPHK2 inhibition in the abundance of genes involved in lung tumor growth or suppression in tissues obtained from SCID mice treated with ABC294640 compared to vehicle were measured by qPCR using Superarray. **(B-C)** Increase in TCF21 mRNA in response to SPHK2 **(B)** (n=3,  $*P=0.016$ ) or hTERT (n=3,  $*P=0.024$ ) **(C)** knockdown using shRNAs in A549 cells was measured by qPCR. ShRNA-mediated knockdown of SPHK2 or hTERT (lower panels in **B** and **C**, respectively) were confirmed by qPCR in A549 cells compared to Scr-shRNA-transfected controls. Data are means  $\pm$  SD from three independent experiments, analyzed by student's t-test (n=3,  $*P=0.038$ ). **(D)** Effects of ectopic expression of WT-hTERT or hTERT<sup>D684A</sup> on TCF21 mRNA in response to shRNA-mediated knockdown of SPHK2 compared to vector-and/or Scr-shRNA-transfected control A549 cells were measured by qPCR. Data are means  $\pm$  SD from three independent experiments, analyzed by student's t-test. (n=3,  $*P=0.0481$ ,  $**P=0.0174$ ,  $***P=0.0267$ ) **(E)** Knockdown of TCF21 using shRNA was confirmed in A549 cells in the presence of ABC294640 compared to Scr-transfected controls by qPCR. Data are means  $\pm$  SD from three independent experiments, analyzed by student's t-test (n=3,  $*P=0.029$ ,  $**P=0.035$ ). **(F)** Effects of shRNA-mediated knockdown of TCF21 on caspase 3 activation in the absence/presence of ABC294640 were measured by immunofluorescence using anti-caspase 3 antibody that detects activated caspase 3 in A549 cells. Images were quantified using ImageJ (bottom panel). Data

are means  $\pm$  SD from three independent experiments, analyzed by student's t-test (n=3, \* $P=0.022$ , \*\* $P=0.036$ , \*\*\* $P=0.019$ ). Scale bars represent 100  $\mu\text{m}$ .

**Supplemental Figure 7. Recombinant purified p16 and caspase 3 proteins interact with each other *in vitro*.** (A) Association between recombinant purified p16 with caspase 3 (A) or mutant (pro) caspase 3 (B) was measured using SPR. (B) Purified caspase 3 protein is visualized by SDS-PAGE and Coomassie blue staining.

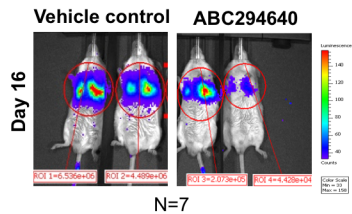
**Fig. S1**

**A**

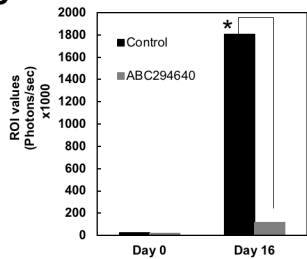


**ABC294640**

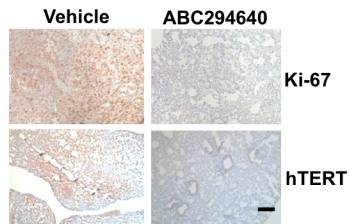
**B**

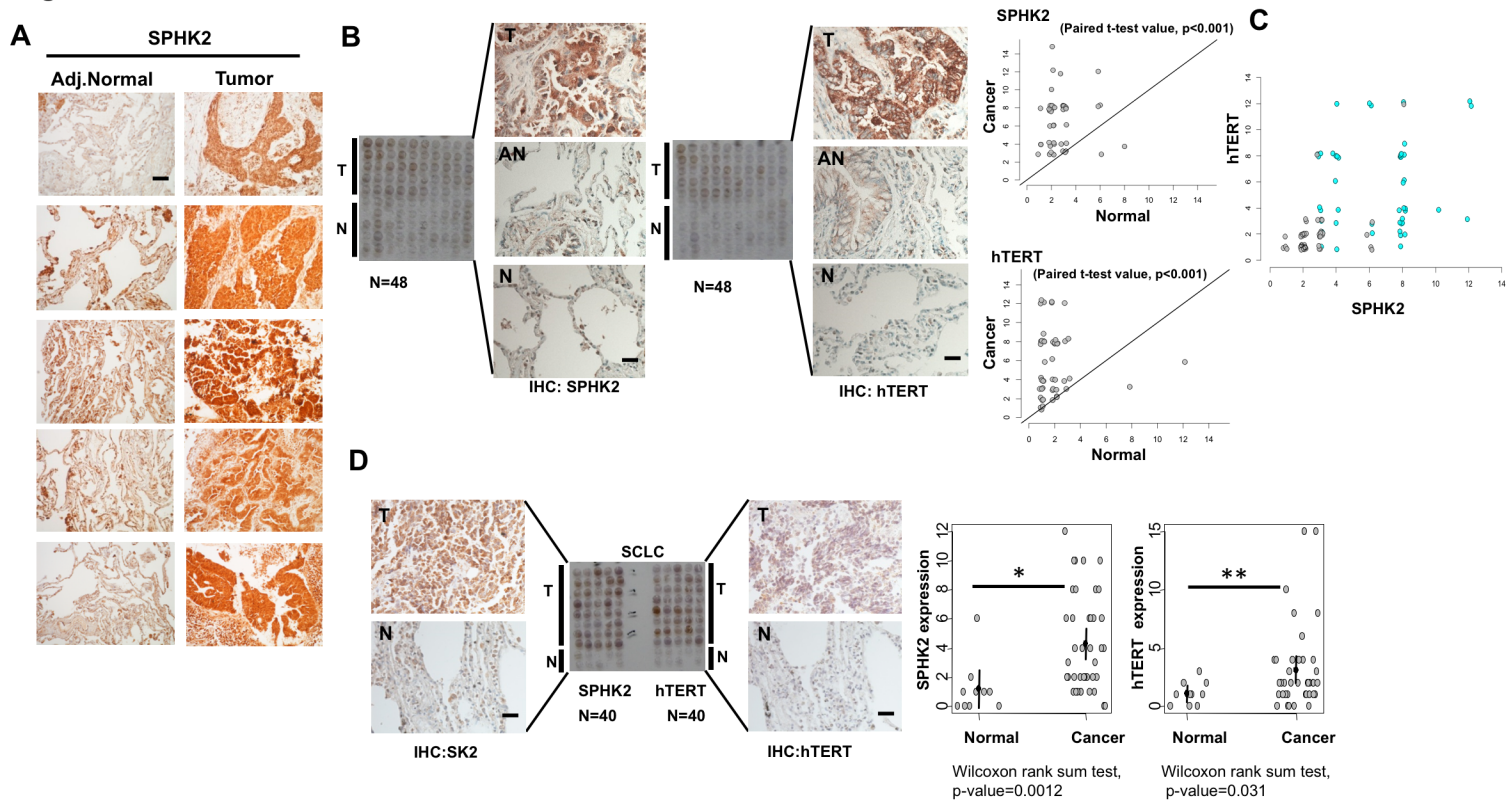


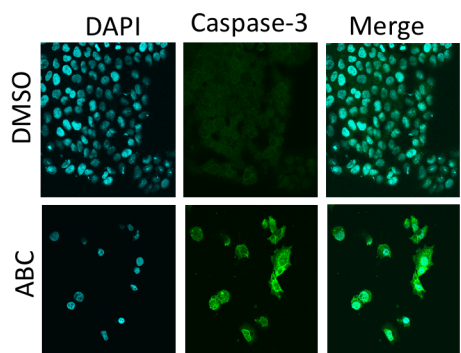
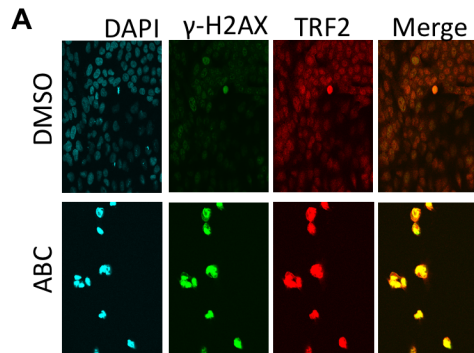
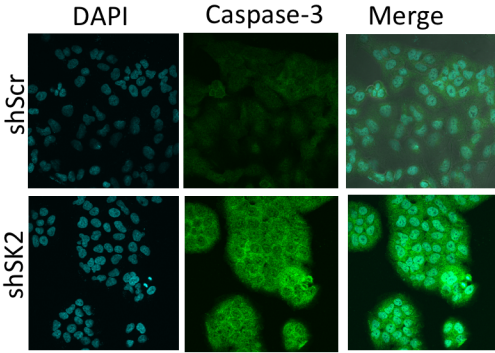
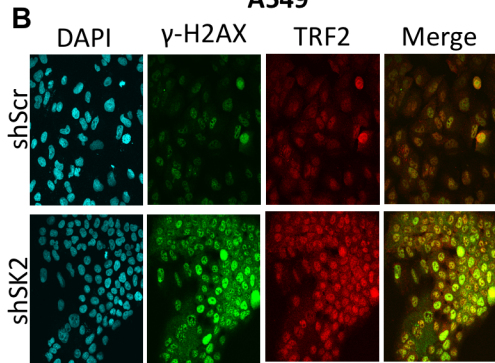
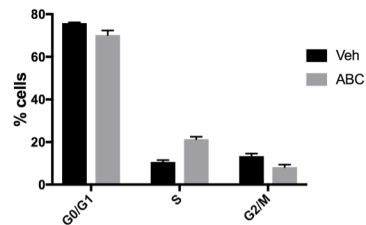
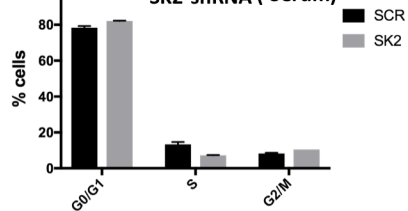
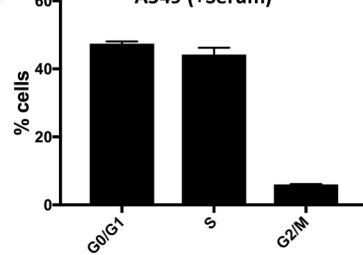
**C**

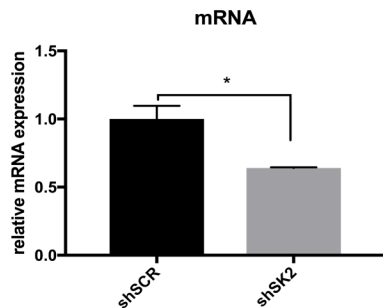


**D**



**Fig. S2**

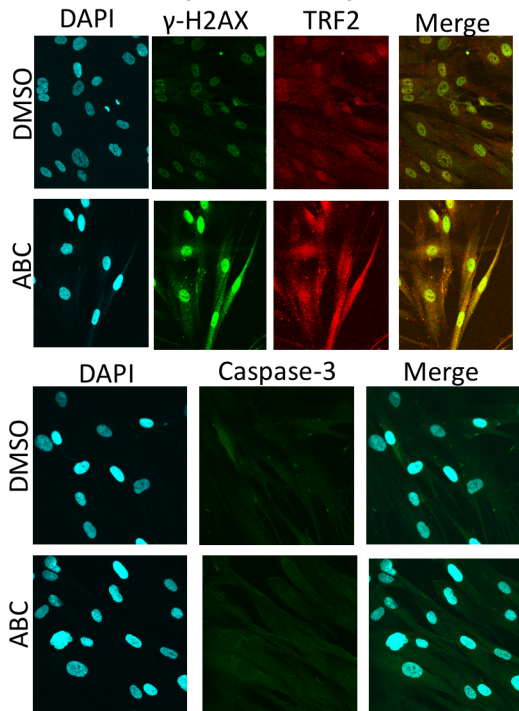
**Fig. S3****A549****A549****C ABC (-Serum)****D SK2-shRNA (-Serum)****E A549 (+Serum)**

**Fig. S4****A****B**

(pmol/ nmol Pi)	shscr	stdev	shSK2	stdev	pvalue
C14-Cer	0.053867	0.045774	0.078244	0.090806	0.254344
C16-Cer	0.388	0.315082	0.578127	0.681898	0.263221
C18-Cer	0.025161	0.018783	0.030254	0.035016	0.480009
C18:1-Cer	0.019249	0.017049	0.027127	0.031359	0.236569
C20-Cer	0.020822	0.012963	0.025347	0.025413	0.417664
C20:1-Cer	0.002473	0.002448	0.004238	0.005355	0.198561
C20:4-Cer	0.000304	0.000589	6.31E-05	2.84E-05	0.376652
C22-Cer	0.131239	0.035028	0.133891	0.079062	0.896334
C22:1-Cer	0.047369	0.022498	0.059177	0.05037	0.349426
C24-Cer	0.728735	0.099656	0.641964	0.121299	0.33781
C24:1-Cer	1.310688	0.367996	1.354093	0.845159	0.837622
C26-Cer	0.142482	0.053084	0.132426	0.055675	0.609873
C26:1-Cer	0.441075	0.043806	0.498921	0.049829	0.153843
dhC16-Cer	0.080372	0.077853	0.151271	0.196085	0.20229
dhSph	0.078683	0.029845	0.096911	0.022955	0.007844
dhSph-1P	0.001065	0.000646	0.000359	0.000152	0.066888
Sph	0.338836	0.178558	0.365334	0.195363	0.058419
Sph-1P	0.000872	0.000296	0.000506	9.33E-05	0.043743

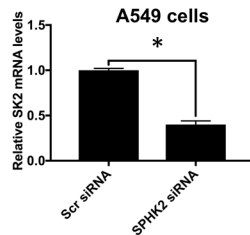
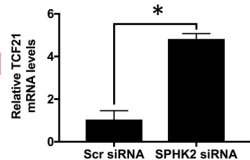
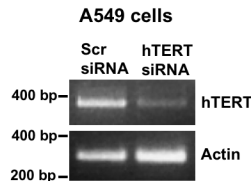
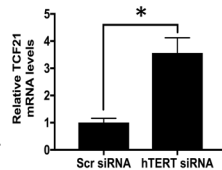
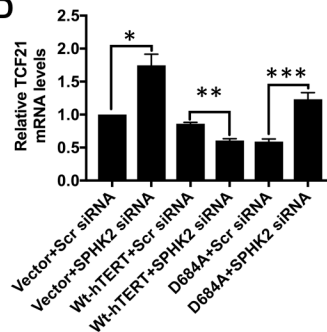
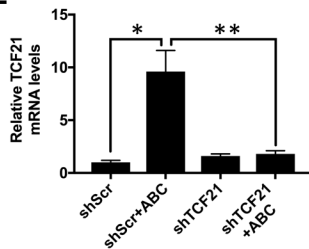
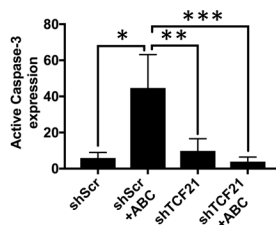
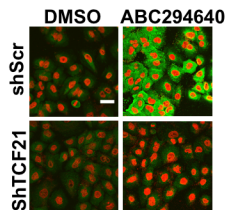
**Fig. S5**

**Primary Non-Cancerous Lung Fibroblasts  
(Generation 2)**



**Fig. S6****A**

Gene	Gene Description	Fold Change
GPM6A	Glycoprotein M6A	21.37
CA4	Carbonic Anhydrase	6.27
CDH13	Cadherin 13/H-Cadherin	6.23
TCF21	Transcription factor 21	5.24
CDKN2A	Cyclin dependent kinase inhibitor 2A (p16)	5.22
CDKN2B	Cyclin dependent kinase inhibitor 2B (p15)	5.05
OPCML	Opioid binding protein/cell adhesion molecule like	4.74
ERBB2	EGFR family	3.17
CXCL13	Chemokine (C-X-C motif) ligand 13	-4.26
MMP9	Matrix metallo peptidase 9	-4.48
CLCA2	Chloride Channel Accessory 2	-8.41

**B****C****D****E****F**

**Fig. S7**

